Supplementary materials for

Black carbon over the South China Sea and in various continental locations in South China

Dui Wu[1], Cheng Wu[2], Biting Liao[1], Huizhong Chen[1], Meng Wu[1], Fei Li[1], Haobo Tan[1], Tao Deng[1], Haiyan Li[1], Dehai Jiang[1], Jian Zhen Yu[2,3,4],

[1] Institute of Tropical and Marine Meteorology, CMA, Guangzhou 510080, China

[2] Division of Environment, Hong Kong University of Science and Technology, Clear Water Bay, Kowloon, Hong Kong, China

[3] Atmospheric Research Centre, Fok Ying Tung Graduate School, Hong Kong University of Science and Technology, Nansha, Guangzhou, China

[4] Department of Chemistry, Hong Kong University of Science and Technology, Clear Water Bay, Kowloon, Hong Kong, China

Correspondence to: Dui Wu (wudui@grmc.gov.cn), Jian Zhen Yu (chjianyu@ust.hk)

I. Supplementary figures

There are a total of 11 supplementary figures. The σ_{abs} data in the dry and rainy seasons are summarized in Figure S1. Diurnal variations of σ_{abs} are shown in Figure S2. Figure S3 shows the weather chart for an example of tropical storm activity on May 17, 2008. Figure S4 shows the histogram of Angstrom Absorption Exponent (AAE) data at Yongxing (YX) in the dry season. AAE variations, along with σ_{abs} at multi wavelengths, are shown in Figure S5. Figure S6 shows frequency distributions and fitted normal distributions of the BC data measured at individual sites. Figures S7 and S8 are enlarged Figures 1 and 2 for better viewing. Figure S9 shows frequency distributions of measured mixing height data by balloon sounding. Individual monthly average wind streams of East Asia in 2008 are shown in Figure S10.

II. Aethalometer data treatment

The 7-channel Aethalometer (model AE31, Magee Scientific, USA) deployed in this study adopts one of the direct measurement techniques similar to the integrating plate method (Lin et al., 1973). Quartz fiber filter tape is used in Aethalometer for aerosol collection at a constant flow rate. Measurement of spectral light transmittance (370, 470, 520, 590, 660, 880, and 950 nm) of the filter tape is conducted at the end of each 5-min measurement cycle. The change of transmittance light intensities signal (I) between each measurement cycle is recorded for attenuation (ATN) calculation, which is defined as follows:

$$ATN = 100 \cdot Ln \frac{I_0}{I} \qquad (1)$$

where the I_0 and I are the intensities of the transmission light through the filter without and with aerosol collected, respectively. When the attenuation of a sample spot on the filter reaches a certain threshold value (125 in this present study) at 370 nm after several cycles of measurements, the Aethalometer will automatically advance the filter tape to a new position for continual measurement. The light absorption coefficient of aerosol on filter can be derived from ATN via following equation:

$$\sigma_{ATN} = ATN \cdot \frac{A}{V} \qquad (2)$$

Where σ_{ATN} is the light absorption coefficient of aerosol on filter, A is the spot area of aerosol deposit, V is the volume of air passing through the filter in each measurement cycle.

Data acquired from filter-based measurement such as Aethalomenter needs carefully correction due to its inherent systemic error (Weingartner et al., 2003; Virkkula et al., 2007; Schmid et al., 2006; Arnott et al., 2005). Coen summarized three known artifacts (Coen et al., 2010), i.e., filter matrix effect, scattering effect and loading effect. The non-linear relationship between σ_{ATN} and σ_{abs} (the light absorption coefficient of suspended aerosol in ambient air) has become a challenge for Aethalomenter, as a linear relationship is assumed by default in its output data. The correction algorithm proposed by Weingartner (Weingartner et al., 2003) was applied in this study to treat the 5-min measurement data:

$$\sigma_{abs} = \frac{\sigma_{ATN}}{C_{ref} \cdot R(ATN)} \qquad (3)$$

where C_{ref} is the constant representing the correction for matrix effect, *R(ATN)* is an function of ATN to correct for the loading effect, which is shown in Eq. (3).

$$R(ATN) = \left(\frac{1}{f} - 1\right) \frac{\ln(ATN\%) - \ln(10\%)}{\ln(50\%) - \ln(10\%)} + 1 \qquad (4)$$

The underlying idea is to first correct all σ_{ATN} to $\sigma_{10\%}$, which then can be corrected into σ_{abs} values through the calibration factor C_{ref}. C_{ref} =3.48 was applied in this study and this value was obtained from the slope of the plot of σ_{ATN} by Aethalomenter vs. σ_{abs} by PAS (Photo-Acoustic Spectrometer) during a comparison study in Pearl River Delta region (Wu et al., 2009). This value is higher but similar to those reported in literature: 2.13 by Weingartner (Weingartner et al., 2003) and 1.9 by Bodhaine (Bodhaine, 1995). The f value in Eq. (4) depends on aerosol types and their mixing state, which is determined through chamber studies (Weingartner et al., 2003). A previous study in the PRD found that soot particles are mainly externally mixed in this region (Cheng et al., 2006). Therefore, corresponding f values are chosen from Weingarthner's study.

The following criteria were applied in data treatment to screen out the invalid data points: (1) AAE should be in the range of 0.5 to 6; (2) data must be available in all seven wavelengths

References

Arnott, W. P., Hamasha, K., Moosmuller, H., Sheridan, P. J., and Ogren, J. A.: Towards aerosol light-absorption measurements with a 7-wavelength Aethalometer: Evaluation with a photoacoustic instrument and 3-wavelength nephelometer, Aerosol Sci Tech, 39, 17-29, Doi 10.1080/027868290901972, 2005.

Bodhaine, B. A.: Aerosol Absorption-Measurements at Barrow, Mauna-Loa and the South-Pole, J Geophys Res-Atmos, 100, 8967-8975, 1995.

Cheng, Y. F., Eichler, H., Wiedensohler, A., Heintzenberg, J., Zhang, Y. H., Hu, M., Herrmann, H., Zeng, L. M., Liu, S., Gnauk, T., Bruggemann, E., and He, L. Y.: Mixing state of elemental carbon and non-light-absorbing aerosol components derived from in situ particle optical properties at Xinken in Pearl River Delta of China, J Geophys Res-Atmos, 111, -, Artn D20204, Doi 10.1029/2005jd006929, 2006.

Coen, M. C., Weingartner, E., Apituley, A., Ceburnis, D., Fierz-Schmidhauser, R., Flentje, H., Henzing, J. S., Jennings, S. G., Moerman, M., Petzold, A., Schmid, O., and Baltensperger, U.: Minimizing light absorption measurement artifacts of the Aethalometer: evaluation of five correction algorithms, Atmos Meas Tech, 3, 457-474, 2010.

Hansen, A. D. A., Rosen, H., and Novakov, T.: The Aethalometer - an Instrument for the Real-Time Measurement of Optical-Absorption by Aerosol-Particles, Science of The Total Environment, 36, 191-196, Doi: 10.1016/0048-9697(84)90265-1, 1984.

Lin, C.-I., Baker, M., and Charlson, R. J.: Absorption Coefficient of Atmospheric Aerosol: a Method for Measurement, Appl. Opt., 12, 1356-1363, 1973.

Schmid, O., Artaxo, P., Arnott, W. P., Chand, D., Gatti, L. V., Frank, G. P., Hoffer, A., Schnaiter, M., and Andreae, M. O.: Spectral light absorption by ambient aerosols influenced by biomass burning in the Amazon Basin. I: Comparison and field calibration of absorption measurement techniques, Atmos Chem Phys, 6, 3443-3462, 2006.

Virkkula, A., Makela, T., Hillamo, R., Yli-Tuomi, T., Hirsikko, A., Hameri, K., and Koponen, I. K.: A simple procedure for correcting loading effects of aethalometer data, J Air Waste Manage, 57, 1214-1222, 2007.

Weingartner, E., Saathoff, H., Schnaiter, M., Streit, N., Bitnar, B., and Baltensperger, U.: Absorption of light by soot particles: determination of the absorption coefficient by means of aethalometers, J Aerosol Sci, 34, 1445-1463, Doi 10.1016/S0021-8502(03)00359-8, 2003.

Wu, D., Mao, J. T., Deng, X. J., Tie, X. X., Zhang, Y. H., Zeng, L. M., Li, F., Tan, H. B., Bi, X. Y., Huang, X. Y., Chen, J., and Deng, T.: Black carbon aerosols and their radiative properties in the Pearl River Delta region, Sci China Ser D, 52, 1152-1163, DOI 10.1007/s11430-009-0115-y, 2009.

Yang, M., Howell, S. G., Zhuang, J., and Huebert, B. J.: Attribution of aerosol light absorption to black carbon, brown carbon, and dust in China - interpretations of atmospheric measurements during EAST-AIRE, Atmos Chem Phys, 9, 2035-2050, 2009.

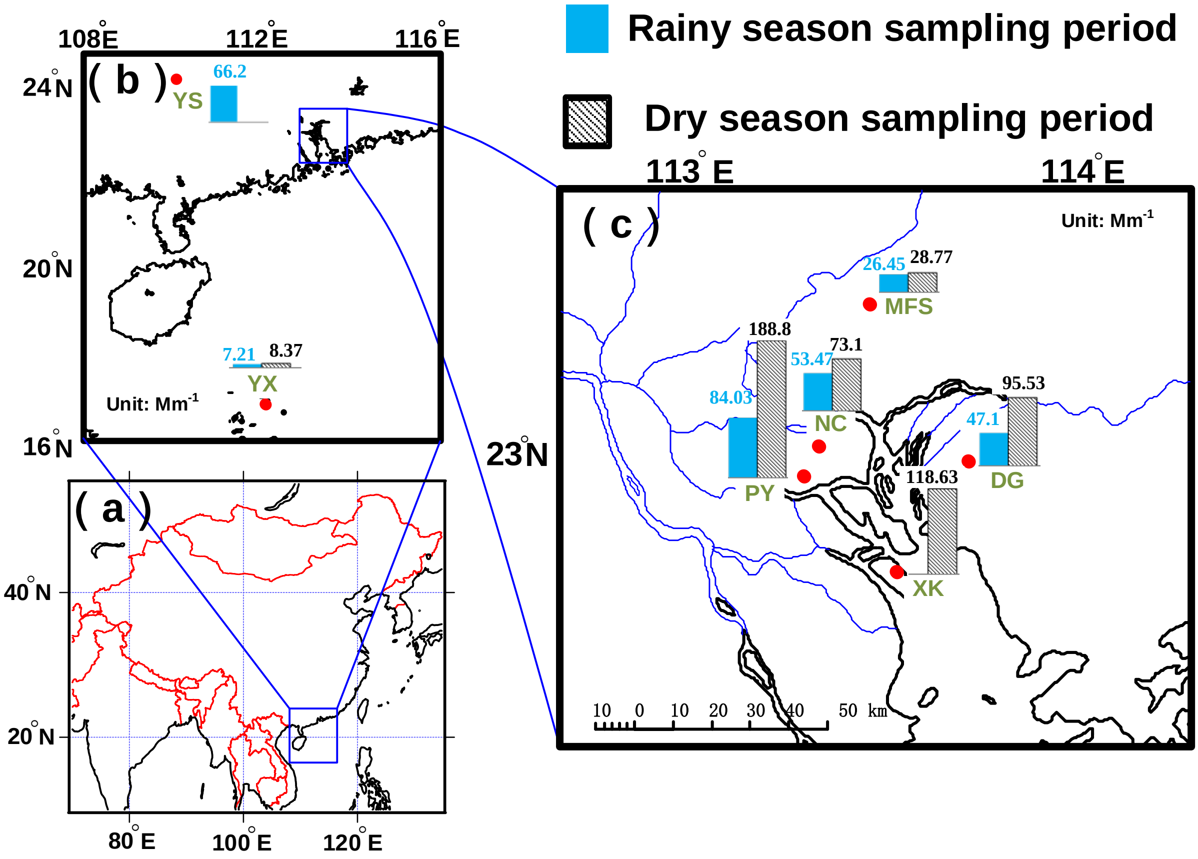

Location	Type	Latitude	Longitude	Elevation (m)
Yongxing island (YX), SCS	Oceanic rural	16.83°N	112.33°E	5.6
Maofengshan (MFS), PRD	Rural	23.33°N	113.48°E	535
Nancun (NC), PRD	Suburban	23.00°N	113.35°E	141
Panyu (PY), PRD	Urban	22.93°N	113.32°E	12
Dongguan (DG), PRD	Suburban	22.97°N	113.73°E	43
Xinken, (XK), PRD	Rural	22.71°N	113.55°E	6.7
Yangshuo (YS), GX	Urban	24.77°N	110.50°E	75

Figure S1. Average light absorption coefficients (σ_{abs}) in Mm^{-1} during rainy and dry seasons across different sampling sites in column plots on the map (column plots in different maps are on the same scale). The enclosed table summarizes the characteristics of sampling sites in this study. **(a)** Location of the study region in China, **(b)** Location of two short-term sites: the oceanic site at Yongxing island (YX) and the urban site Yangshuo (YS). **(c)** Location of the long-term sites in PRD, including Maofengshan (MFS), Nancun (NC), Panyu, (PY), Dongguan (DG), Xinken(XK).

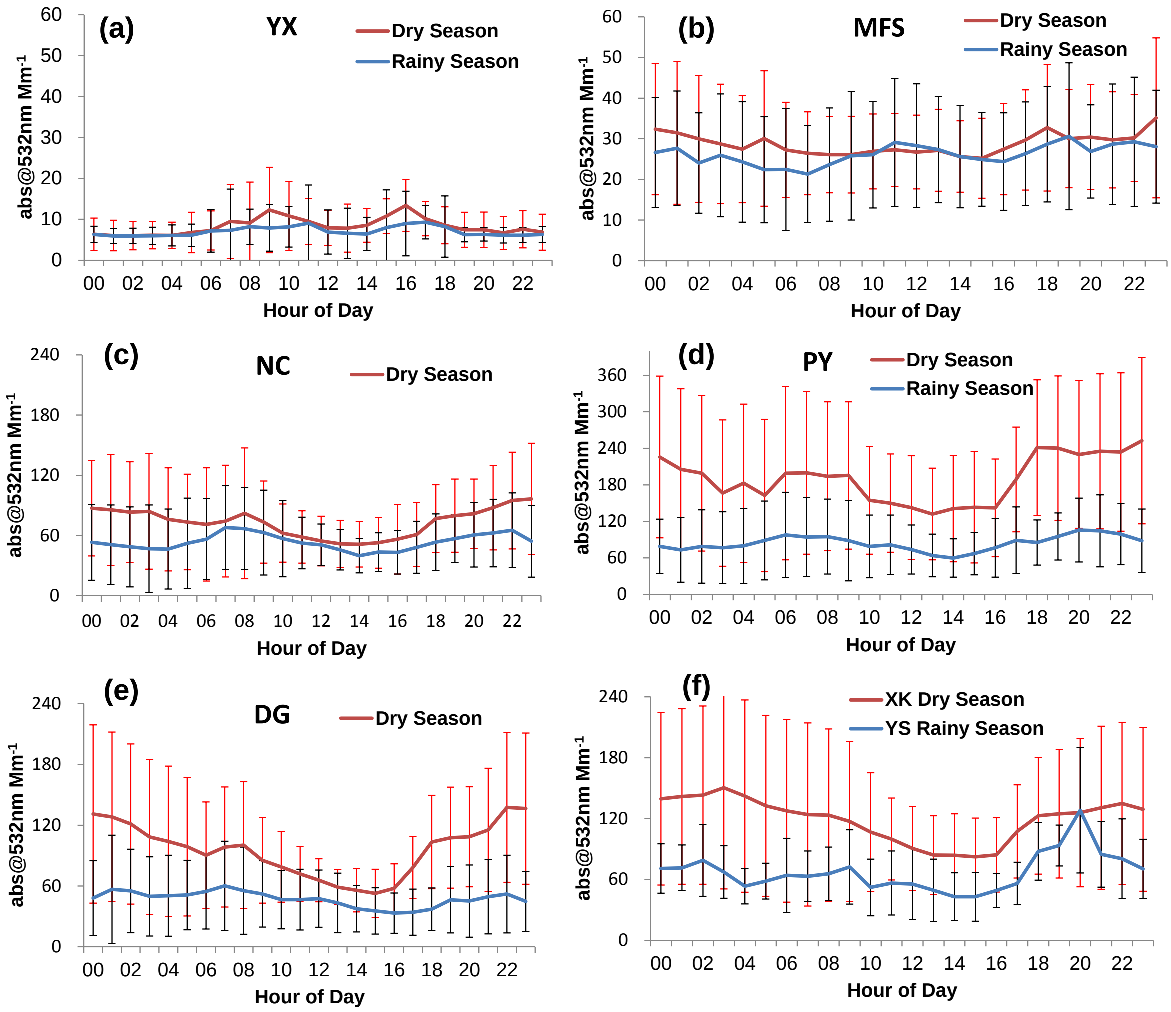

Figure S2. Diurnal variations of absorption coefficients at six monitoring sites in rainy and dry seasons. The sites are **(a)** Maofengshan (MFS), **(b)** Yongxing island (YX), **(c)** Nancun (NC), **(d)** Panyu (PY), **(e)** Dongguan (DG), and **(f)** Xinken (XK) in dry season and Yangshuo (YS) in rainy season.

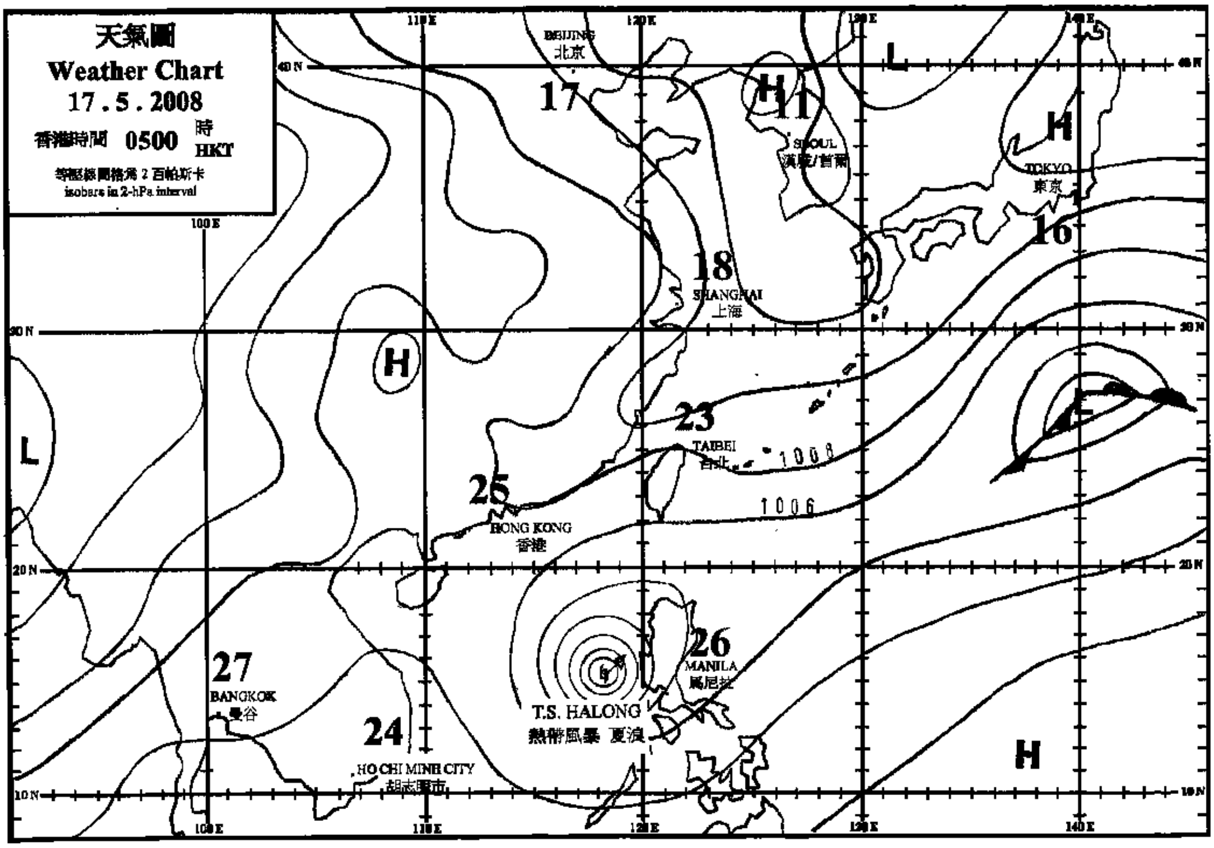

Figure S3. Tropical storm Halong over the South China Sea when approaching Philippines (17 May 2008 5:00)

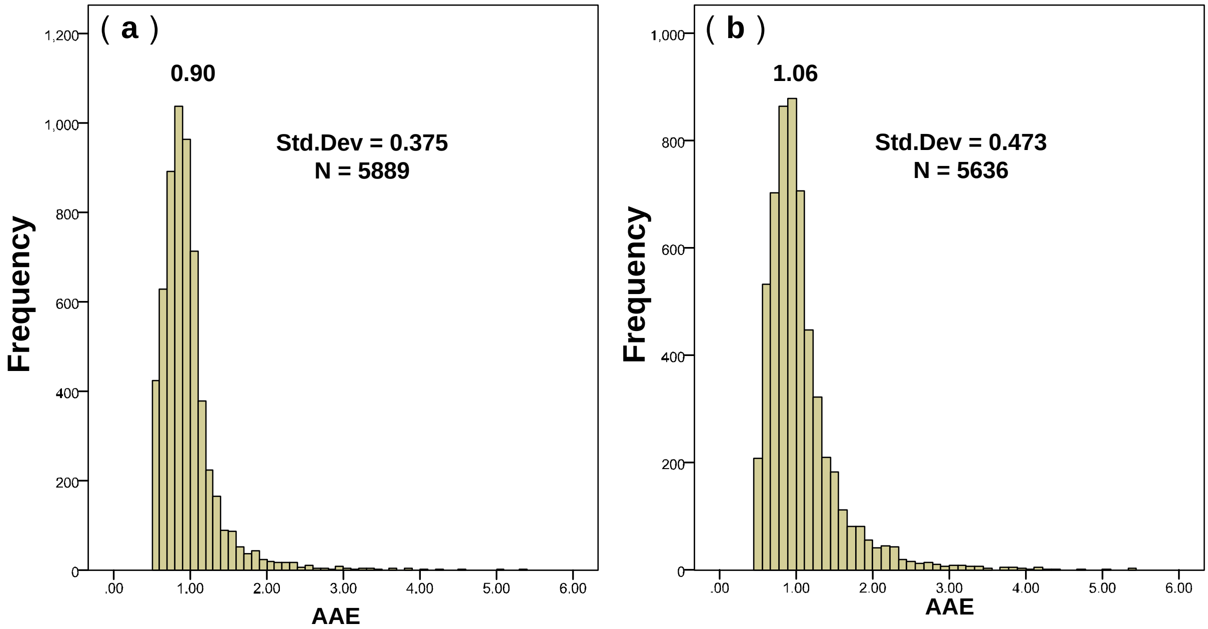

Figure S4. Distribution of Absorption Angstrom Exponent (AAE) values at YX in (a) Rainy season and (b) Dry season.

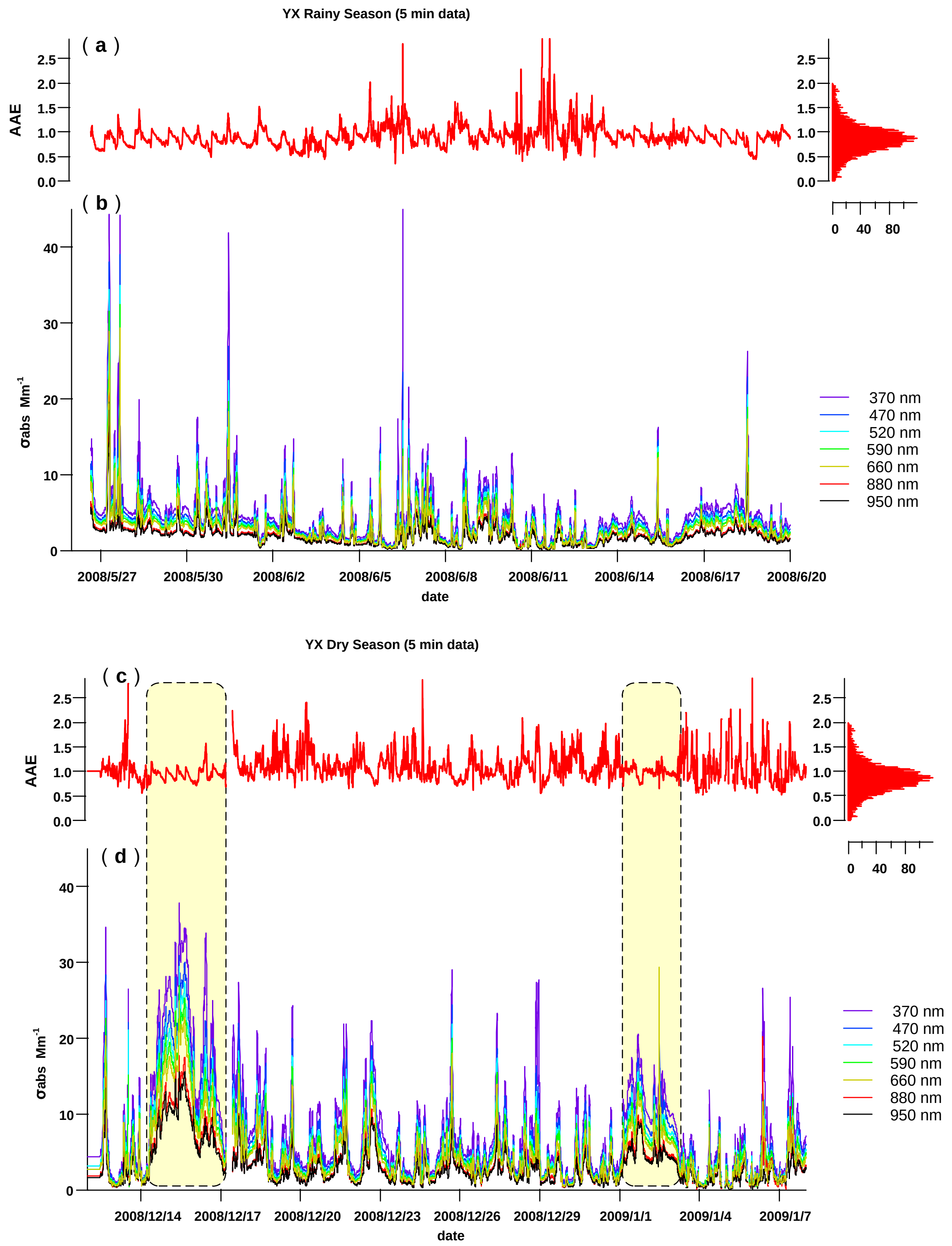

Figure S5. Time series variations (5 min data) of: **(a)** Absorption Angstrom Exponent (AAE) at YX during rainy season; **(b)** σ_{abs} at seven wavelengths at YX during rainy season; (c) AAE at YX during dry season; **(d)** σ_{abs} at seven wavelengths at YX during dry season. The highlighted areas mark two episodic events observed during dry season.

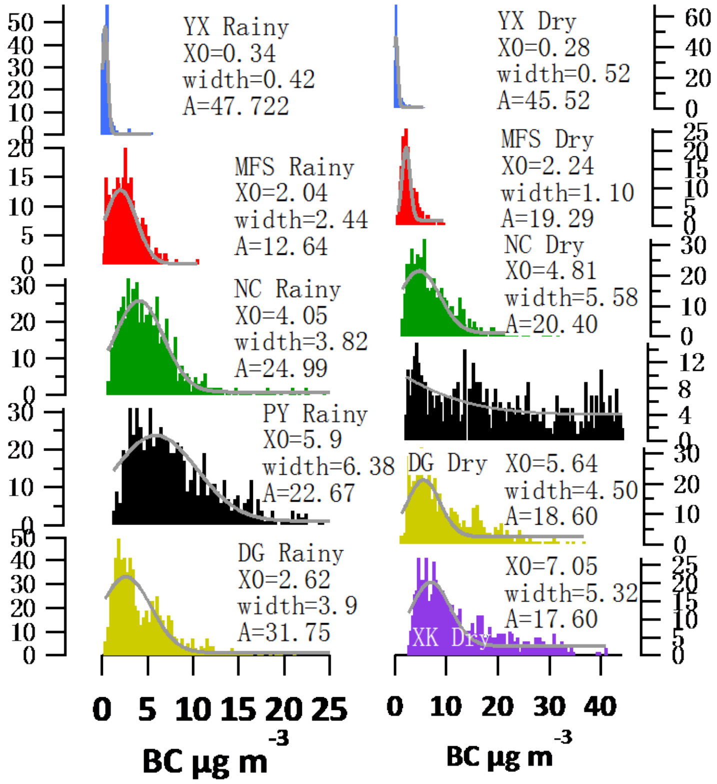

Figure S6 Frequency distributions and fitted normal distributions of the BC data measured at individual sites.

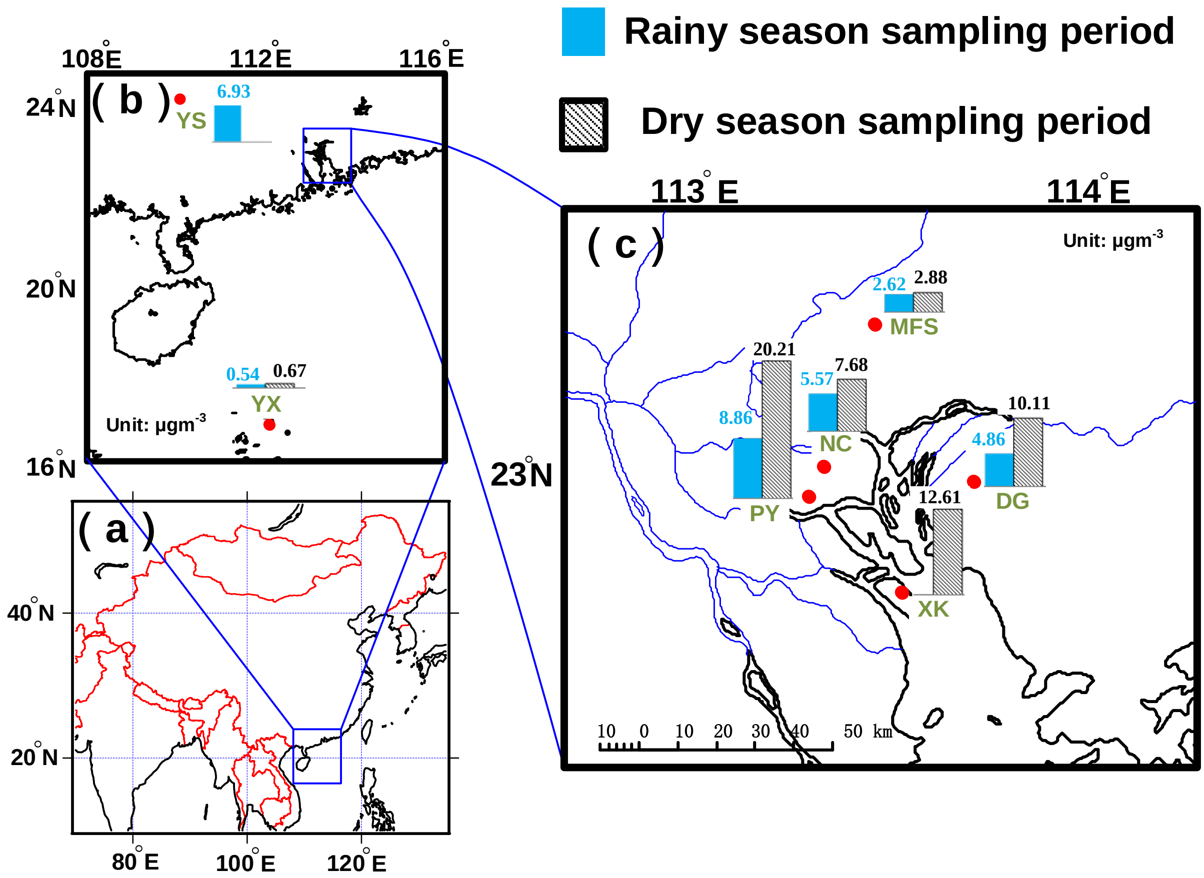

Location	Type	Latitude	Longitude	Elevation (m)
Yongxing island (YX), SCS	Oceanic rural	16.83°N	112.33°E	5.6
Maofengshan (MFS), PRD	Rural	23.33°N	113.48°E	535
Nancun (NC), PRD	Suburban	23.00°N	113.35°E	141
Panyu (PY), PRD	Urban	22.93°N	113.32°E	12
Dongguan (DG), PRD	Suburban	22.97°N	113.73°E	43
Xinken, (XK), PRD	Rural	22.71°N	113.55°E	6.7
Yangshuo (YS), GX	Urban	24.77°N	110.50°E	75

Figure S7. Enlarged Figure 1. Average black carbon concentrations during rainy and dry season sampling periods across different sampling sites in column plots on the map (column plots in different maps are on the same scale and the unit of the associated numbers is μg m^{-3}). The table in the figure summarizes characteristics of the sampling sites in this study. **(a)** Location of the study region in China **(b)** Location of the two short-term sites: oceanic site at Yongxing island (YX) and the urban site Yangshuo (YS). **(c)** Location of the long-term sites in the Pearl River Delta, including Maofengshan (MFS), Nancun (NC), Panyu (PY), Dongguan (DG), and Xinken(XK).

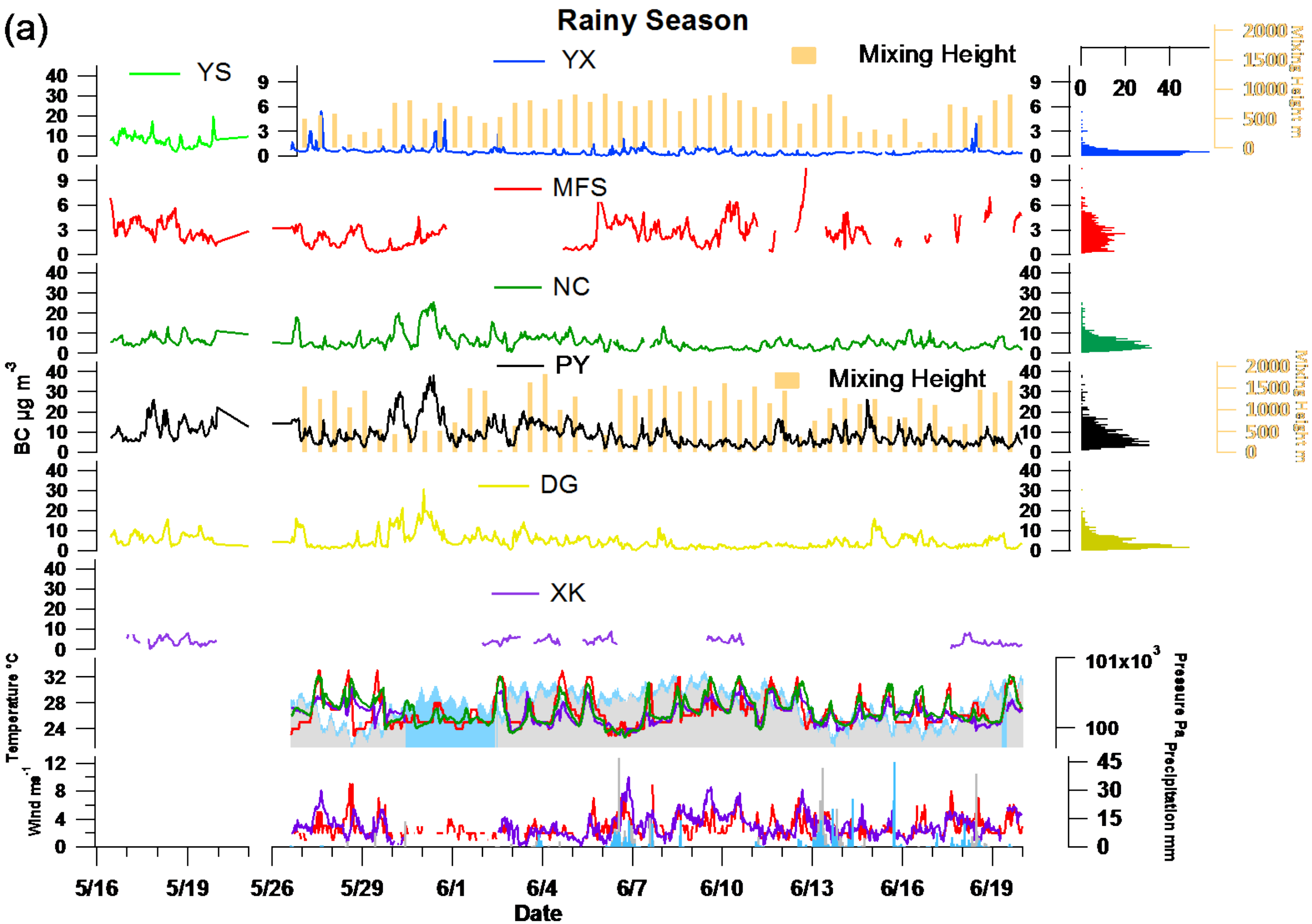

(a)
Rainy Season
YS
YX
Mixing Height
MFS
NC
PY
Mixing Height
DG
XK
BC µg m-3
Temperature °C
Wind ms-1
Pressure Pa
Precipitation mm
Mixing Height m
Date
5/16
5/19
5/26
5/29
6/1
6/4
6/7
6/10
6/13
6/16
6/19

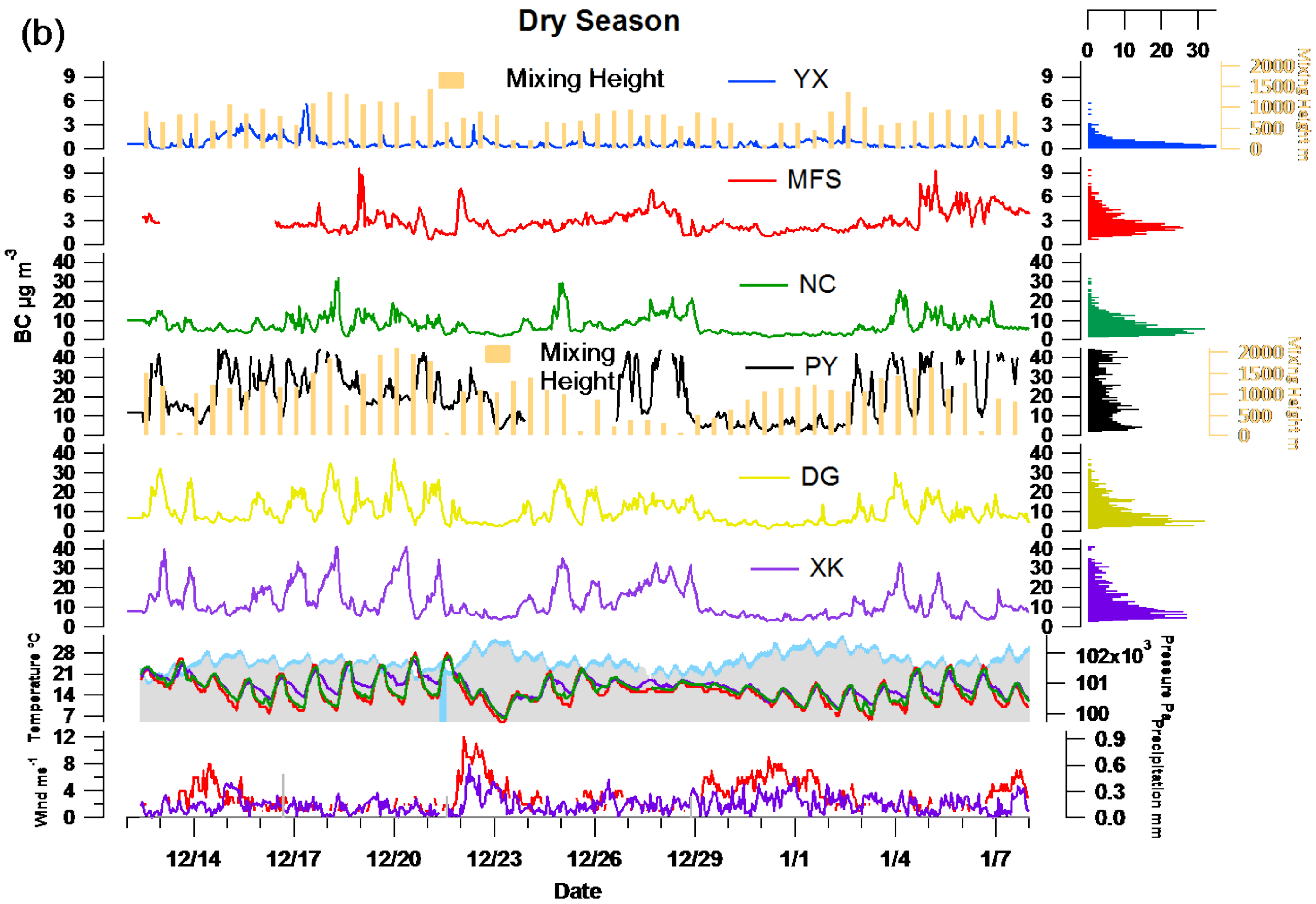

Figure S8. Enlarged Figure 2. Time series of BC hourly concentrations, temperature, atmospheric pressure, wind speed, and precipitation amount in (a) rainy season sampling period (b) dry season sampling period. The bar plots overlaying on the BC plots at YX and PY show the mixing height from balloon measurements. The histograms shown to the right of BC time series are the frequency distributions of BC concentrations. In the temperature time series plots, the red curve is measurements for Baiyun airport, 17 km west to MFS, and is considered to represent meteorological conditions in the northern part of PRD; the green curve is for NC and the purple curve is for XK. In the station pressure plots, the grey areas represent XK and the light blue for NC. In the wind speed plots, red is for the Baiyun airport, purple for XK. In the precipitation plots, grey bars are for XK and light blue for urban Guangzhou.

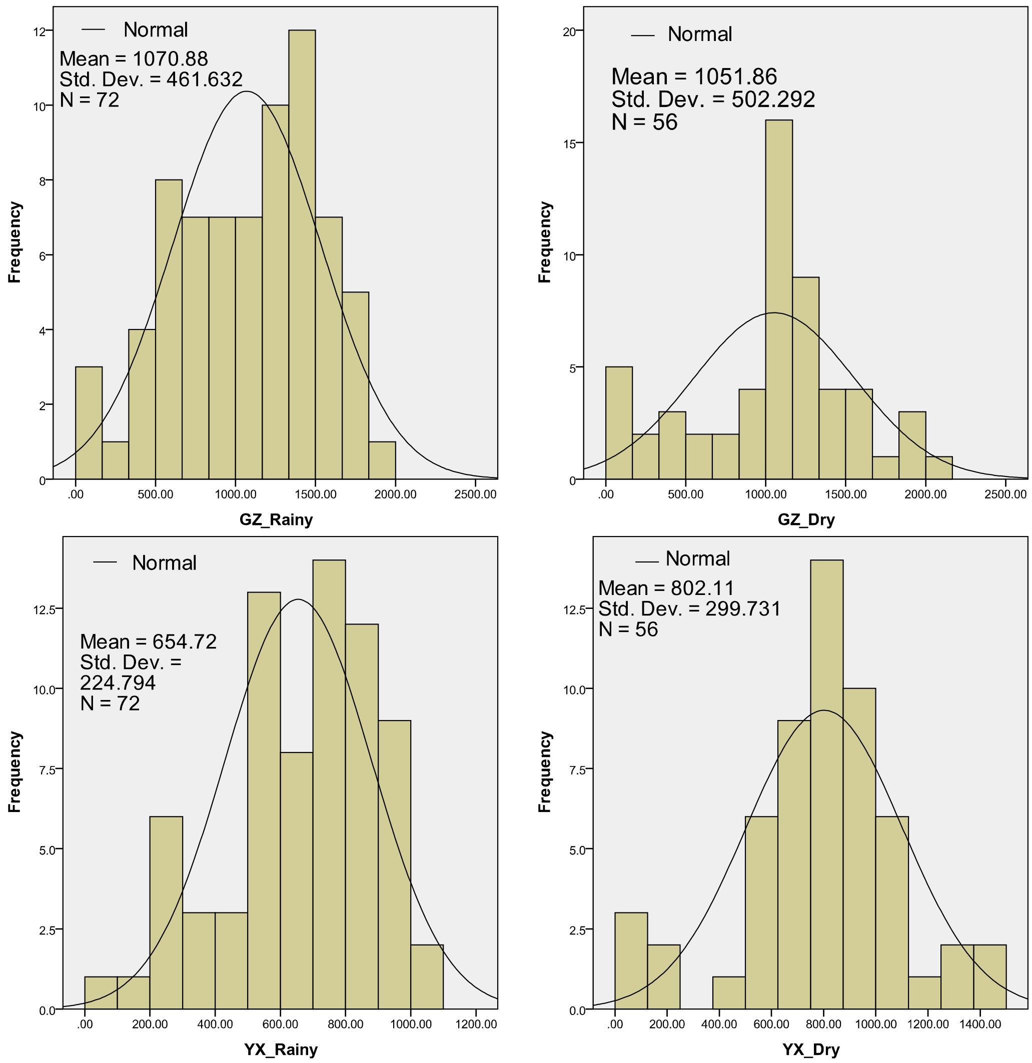

Figure S9. Frequency distribution of measured mixing height data by balloon sounding.

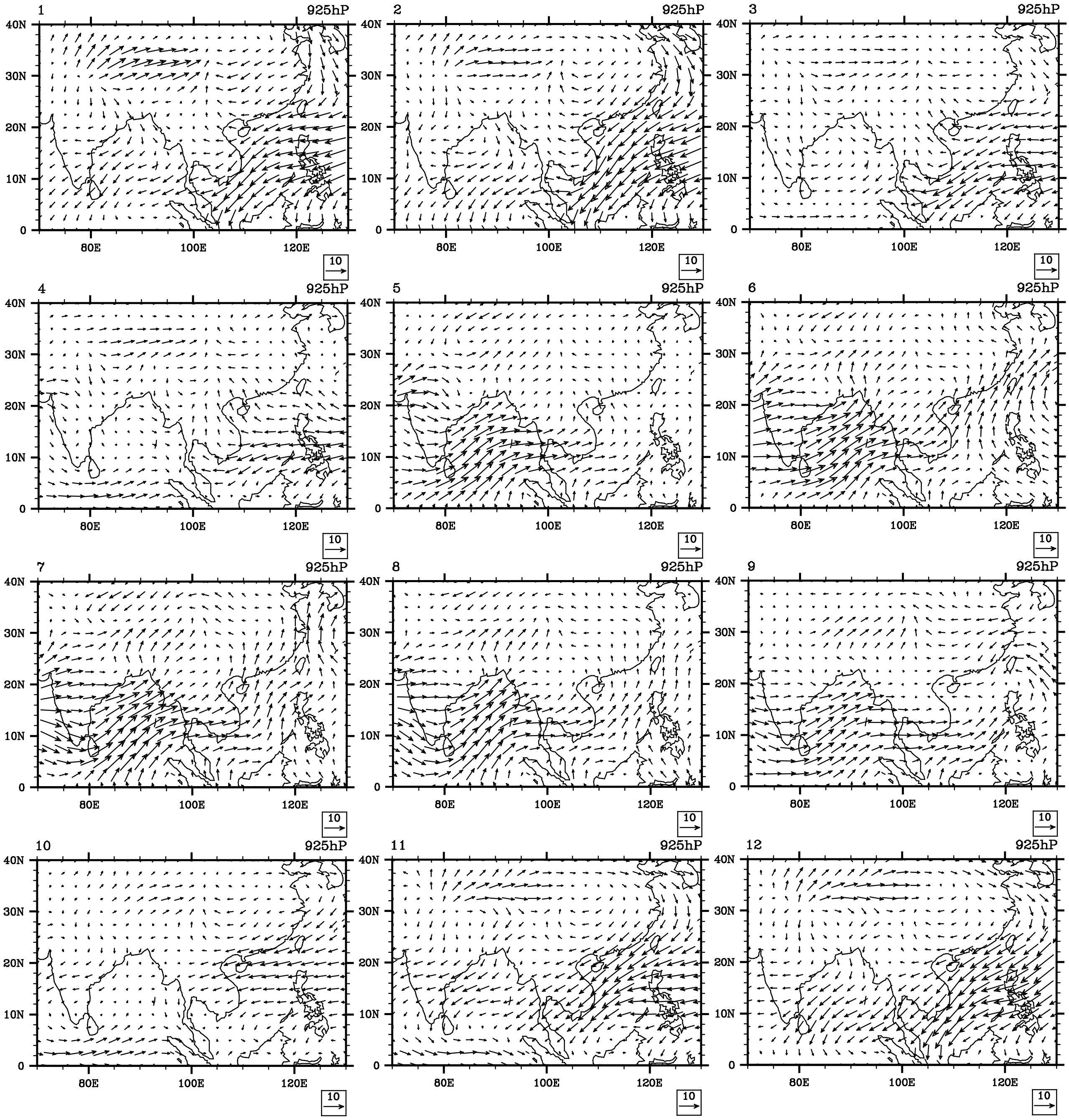

Figure S10 Individual monthly average wind streams of East Asia in 2008

Figure S11 Back trajectories analysis of air masses arriving at MFS, NC, and YX at five different heights (100, 300, 500, 1000, and 1500 m) in the rainy and dry season sampling periods. [The next 30 pages]

MFS Rainy 100m

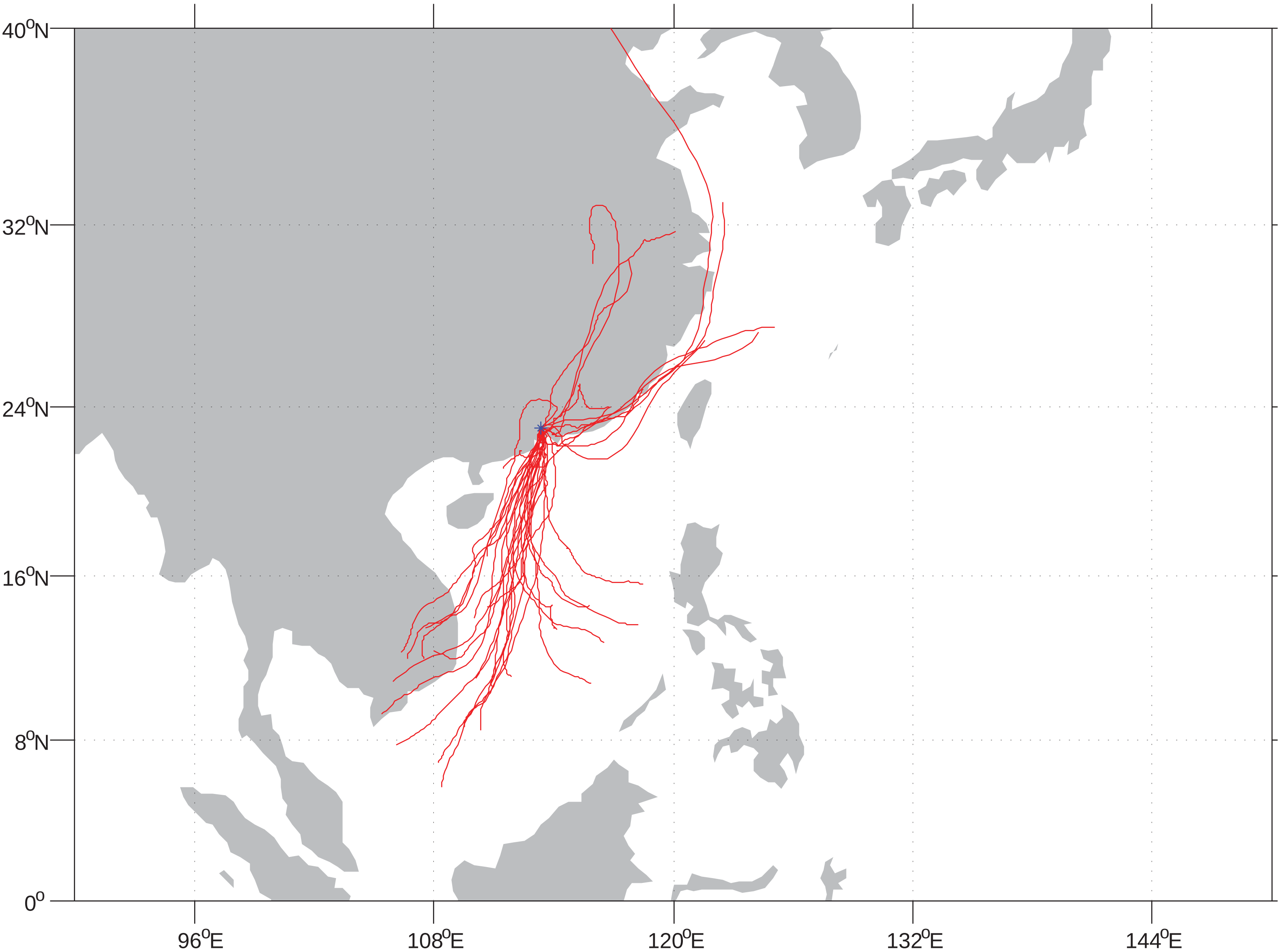

MFS Rainy 300m

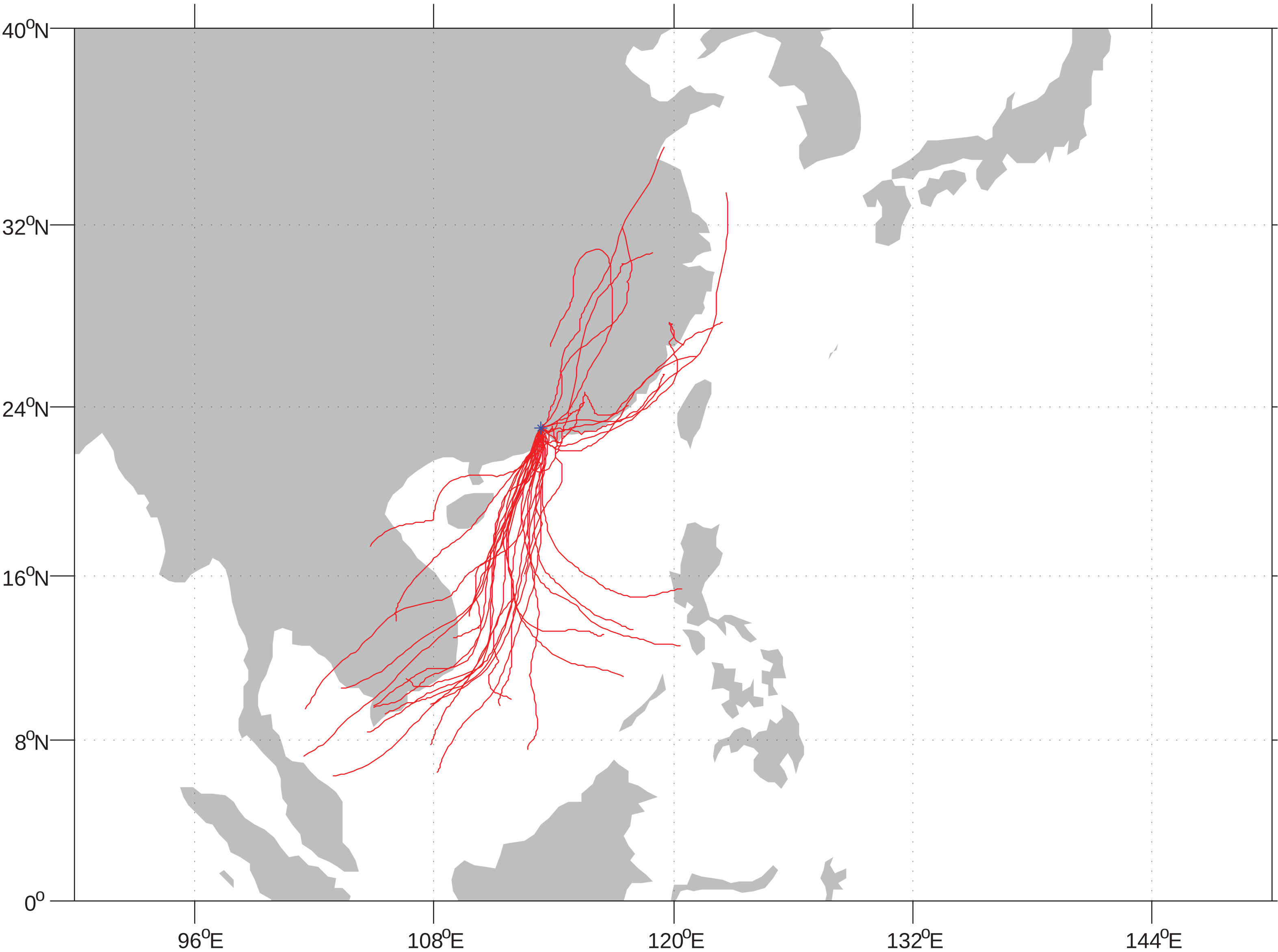

MFS Rainy 500m

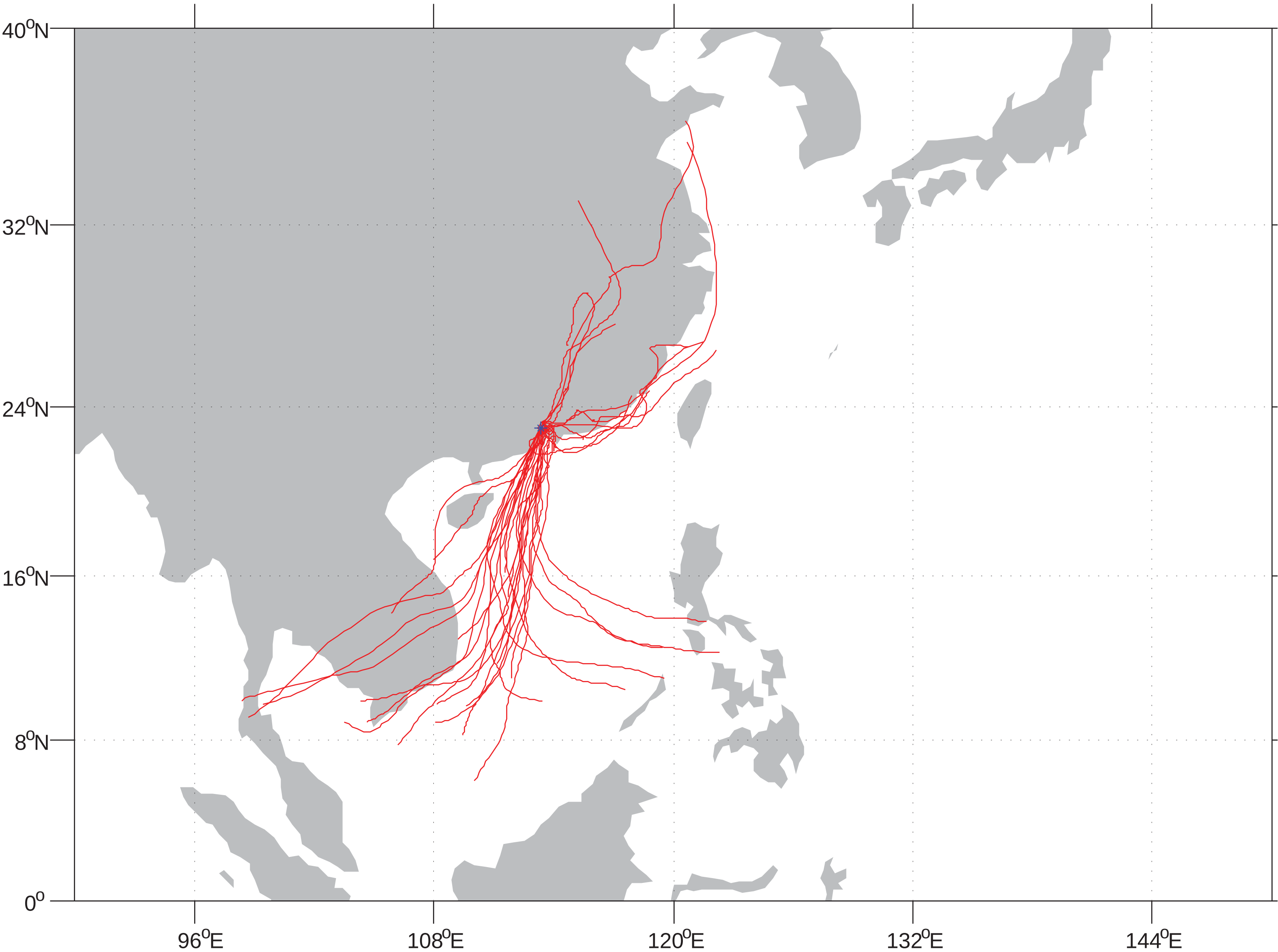

MFS Rainy 1000m

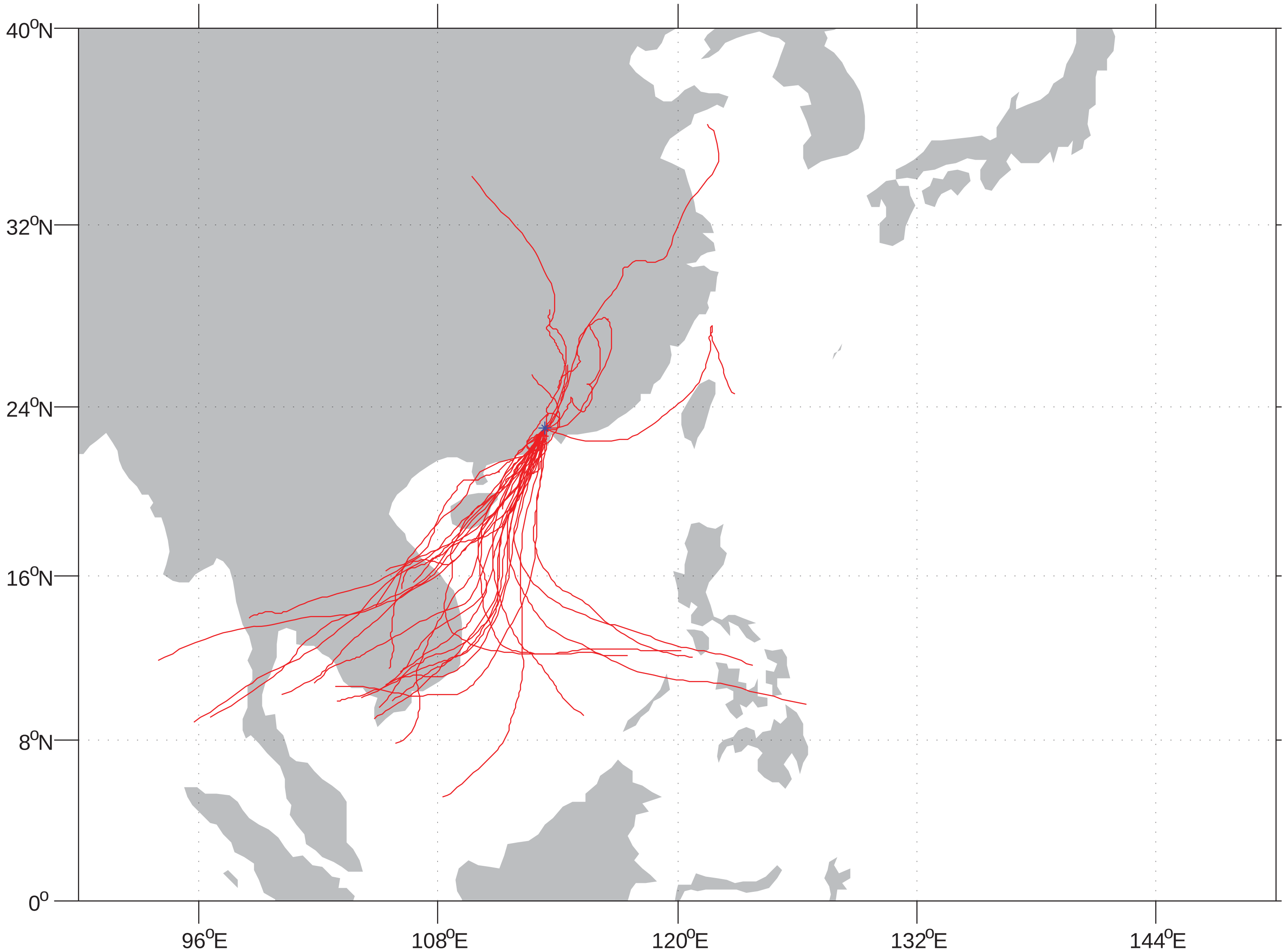

MFS Rainy 1500m

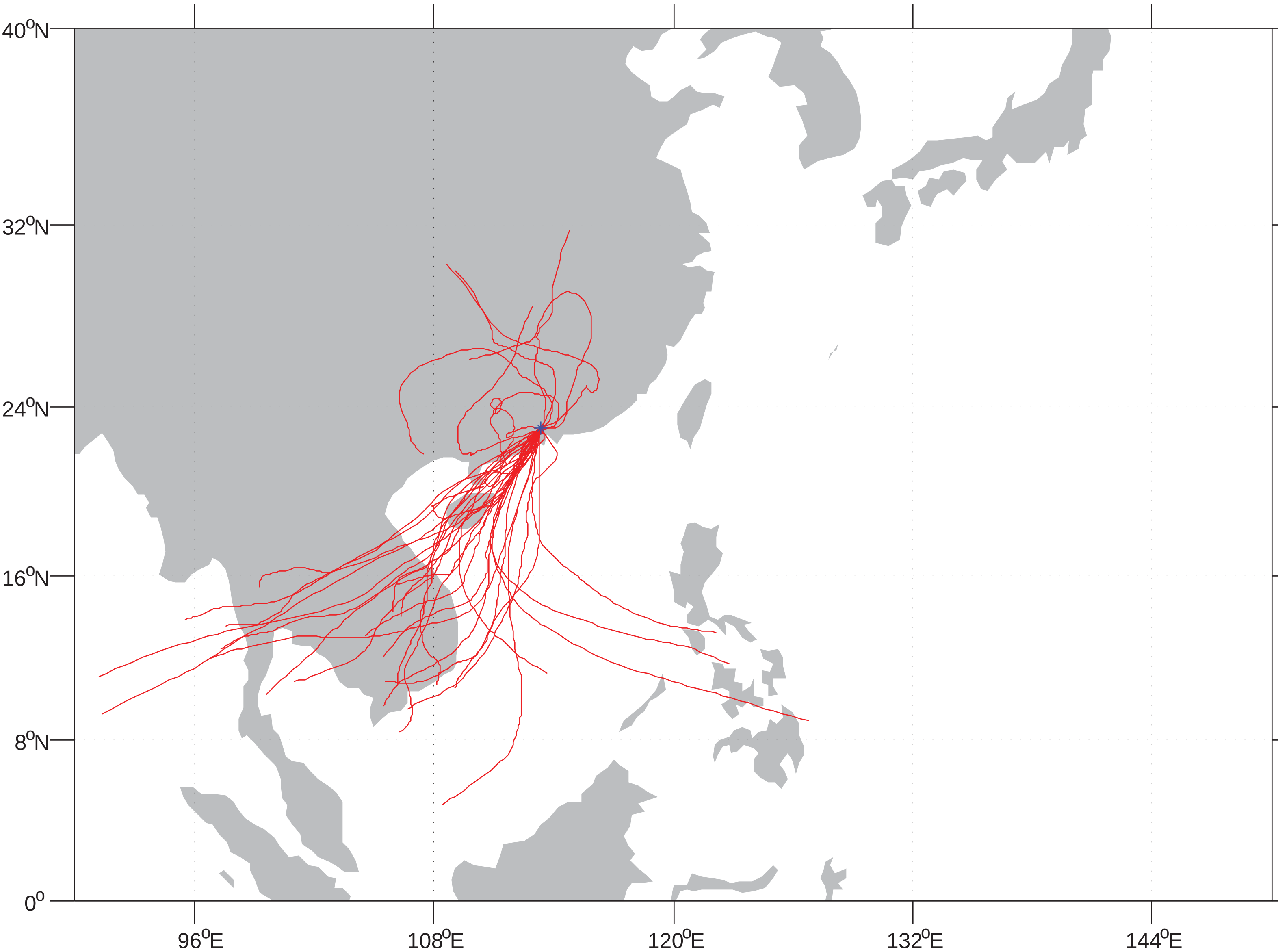

MFS Dry 100m

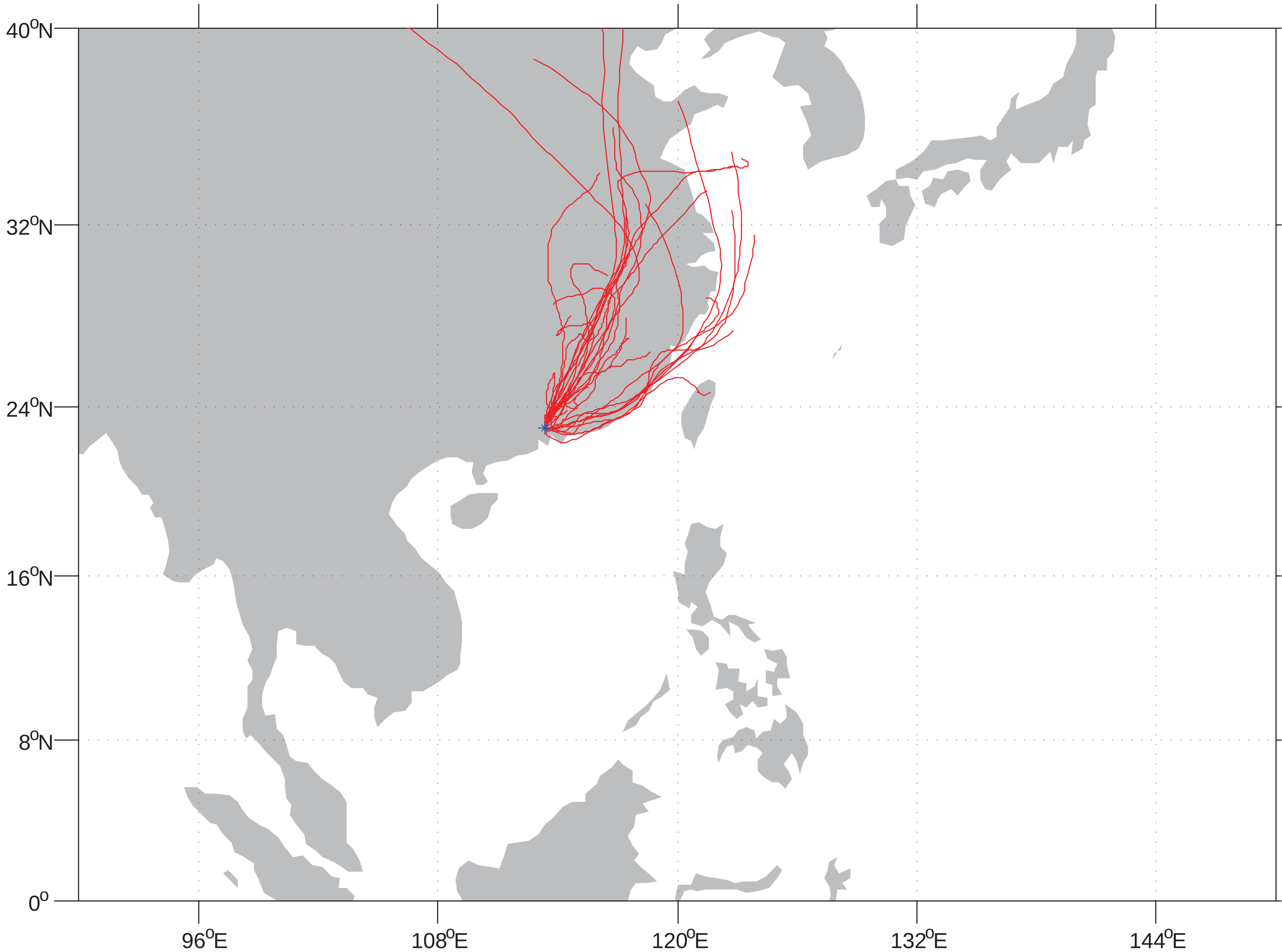

MFS Dry 300m

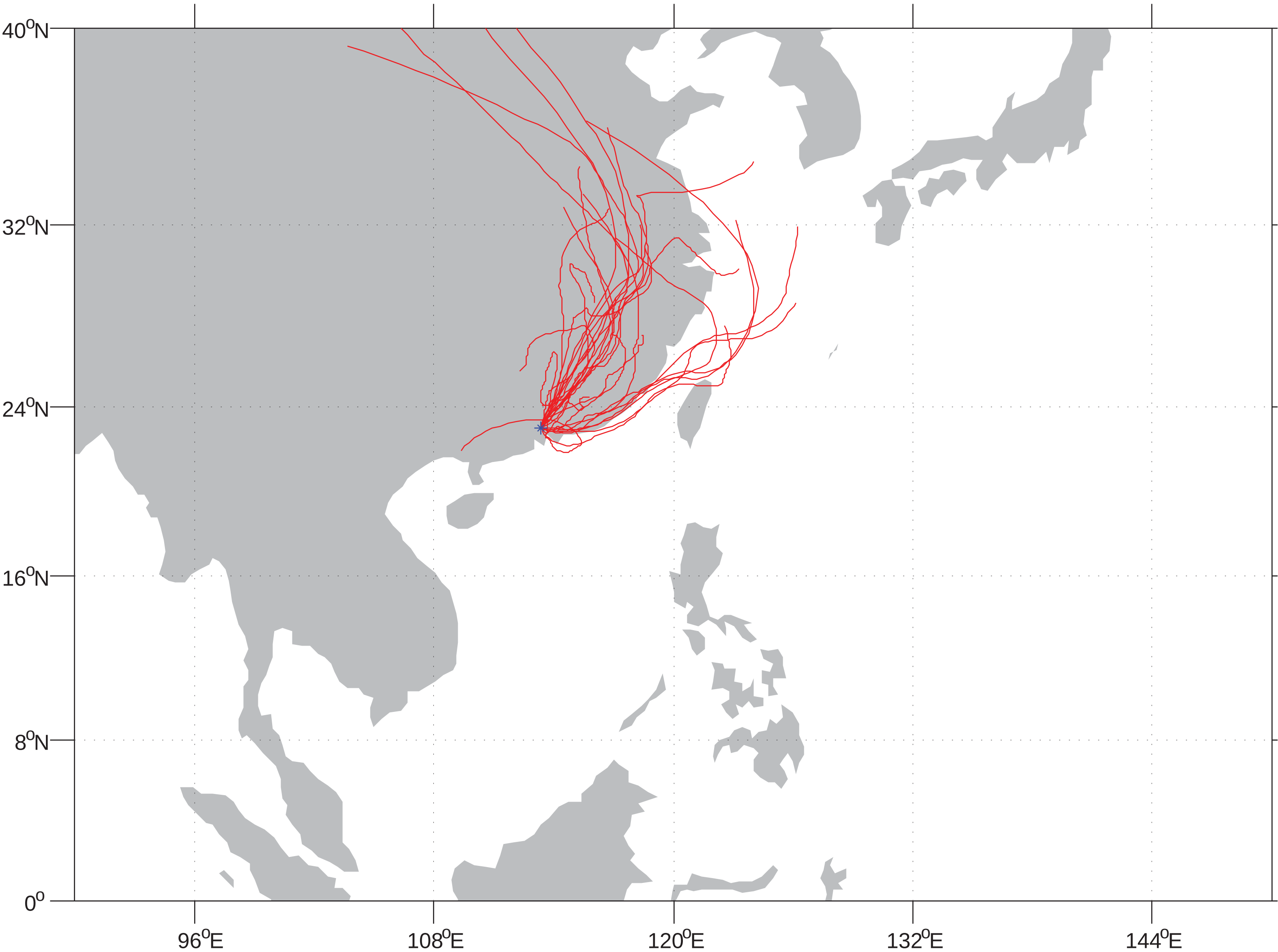

MFS Dry 500m

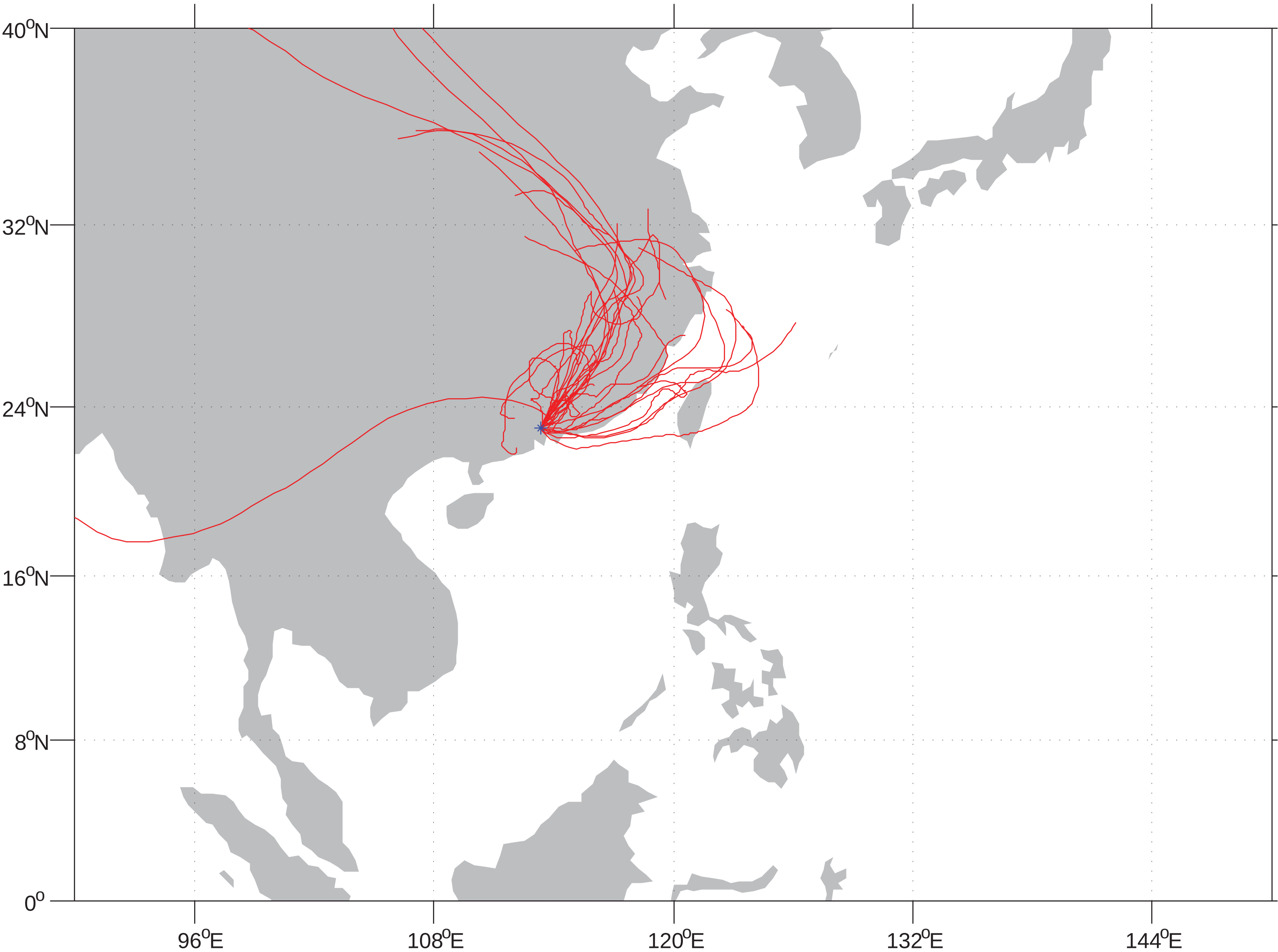

MFS Dry 1000m

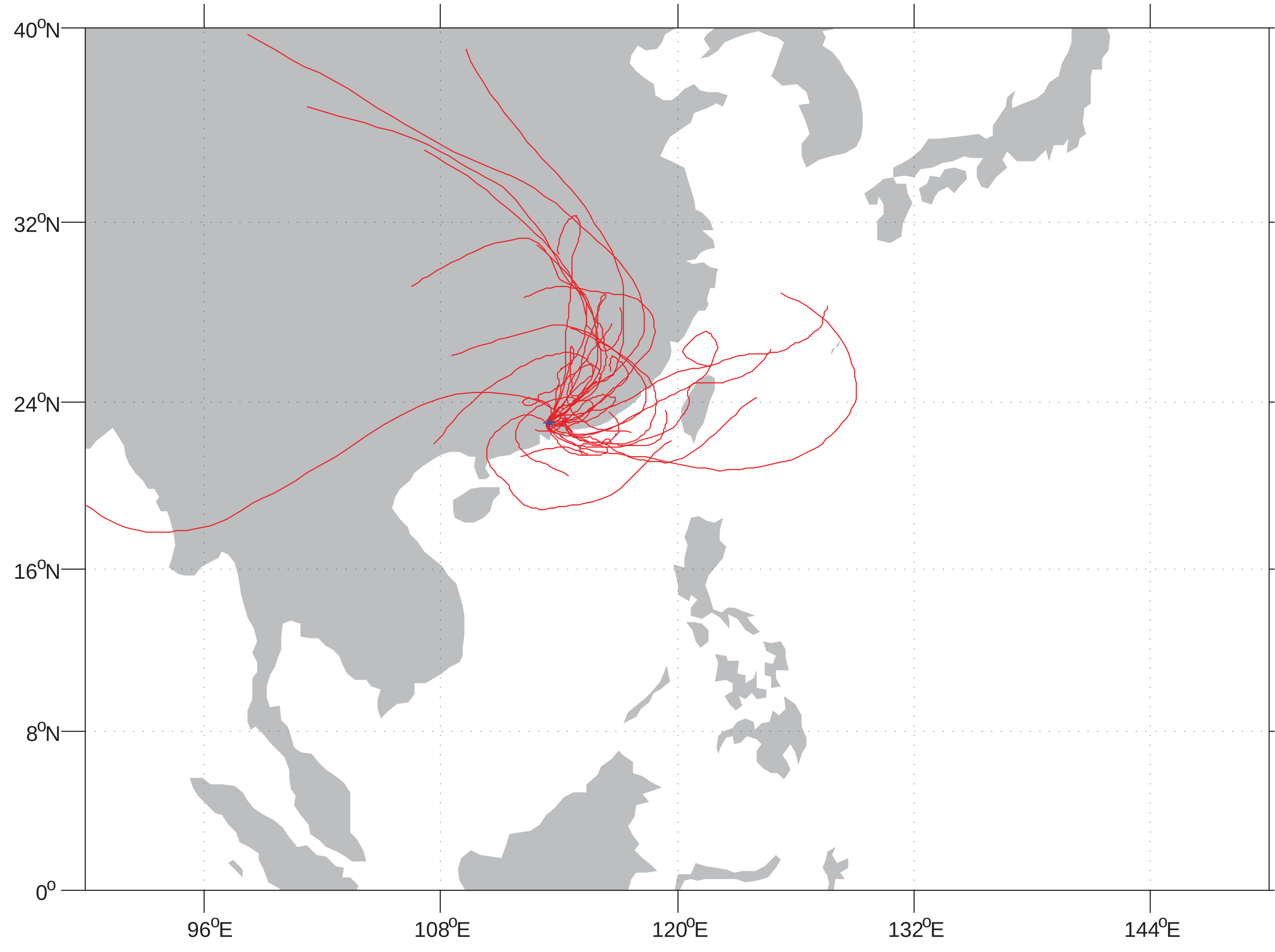

MFS Dry 1500m

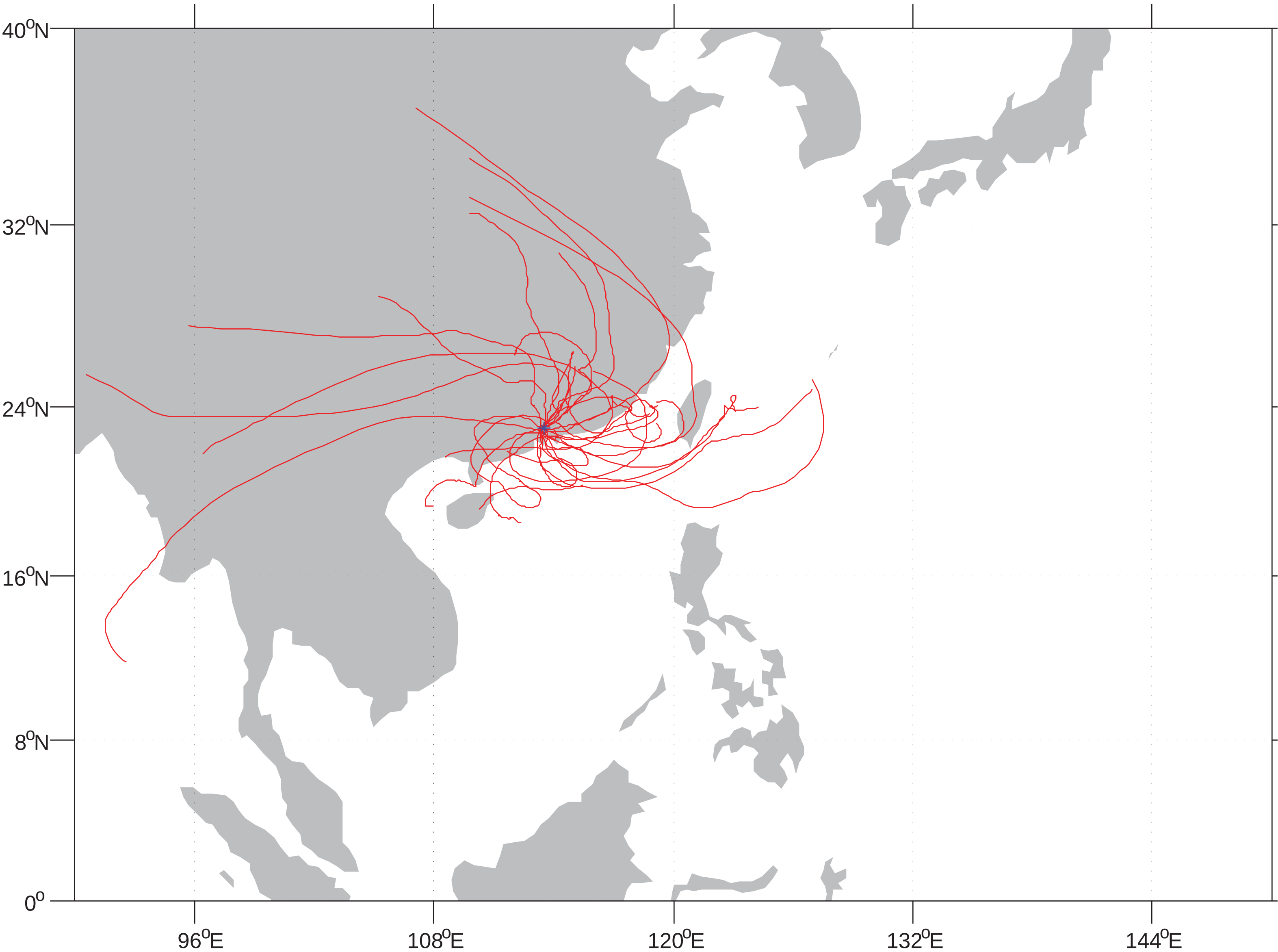

NC Rainy 100m

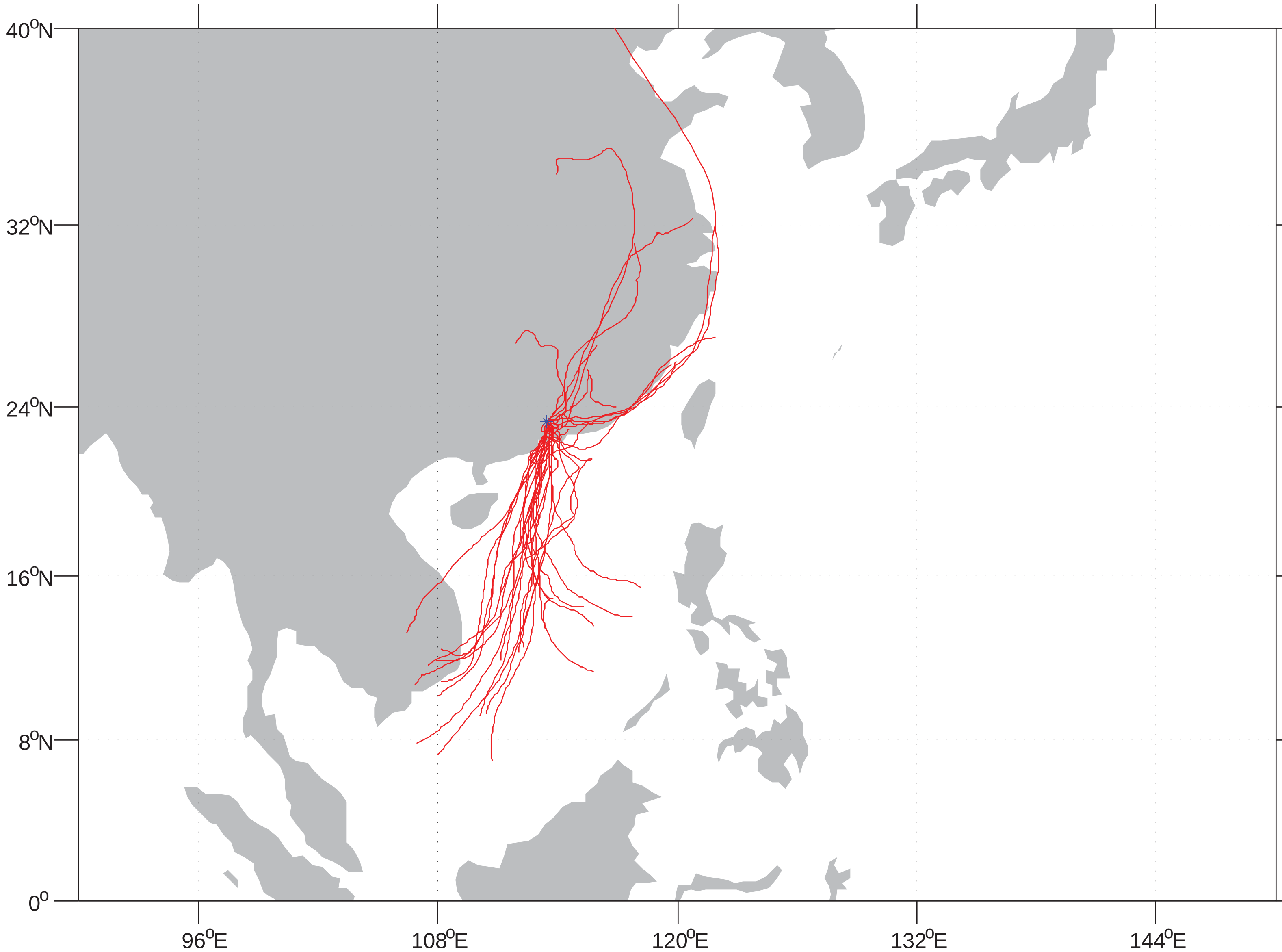

NC Rainy 300m

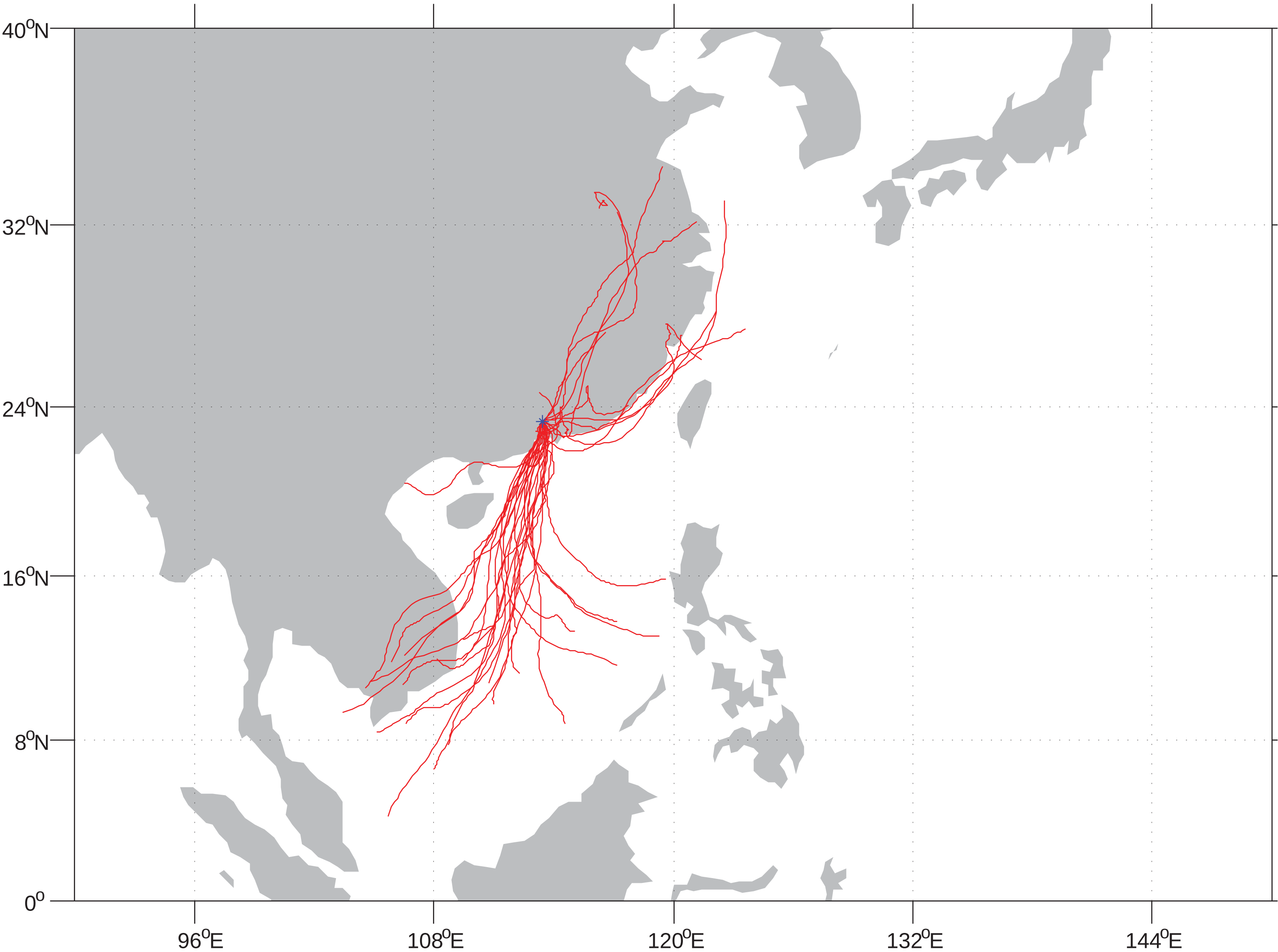

NC Rainy 500m

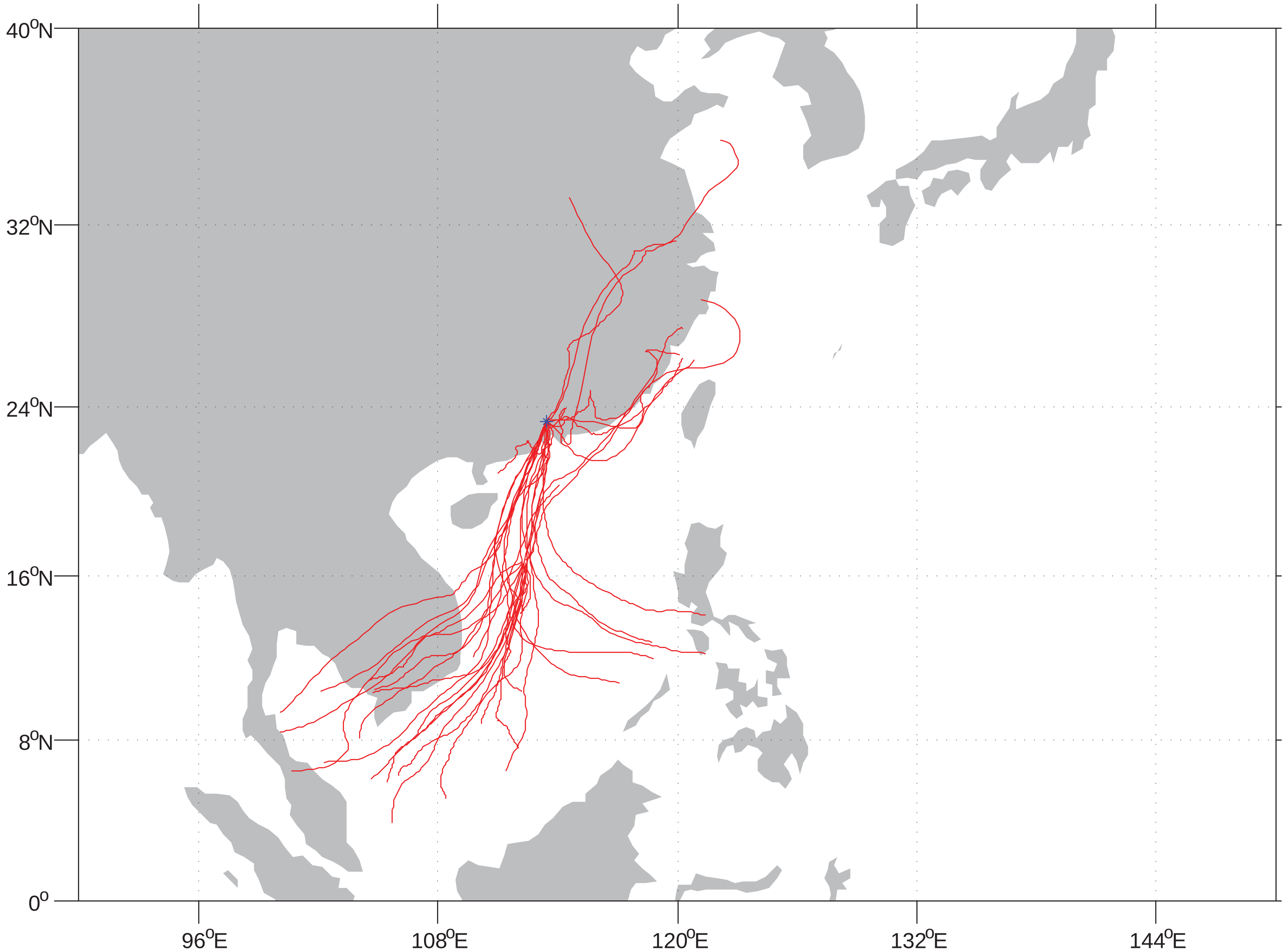

NC Rainy 1000m

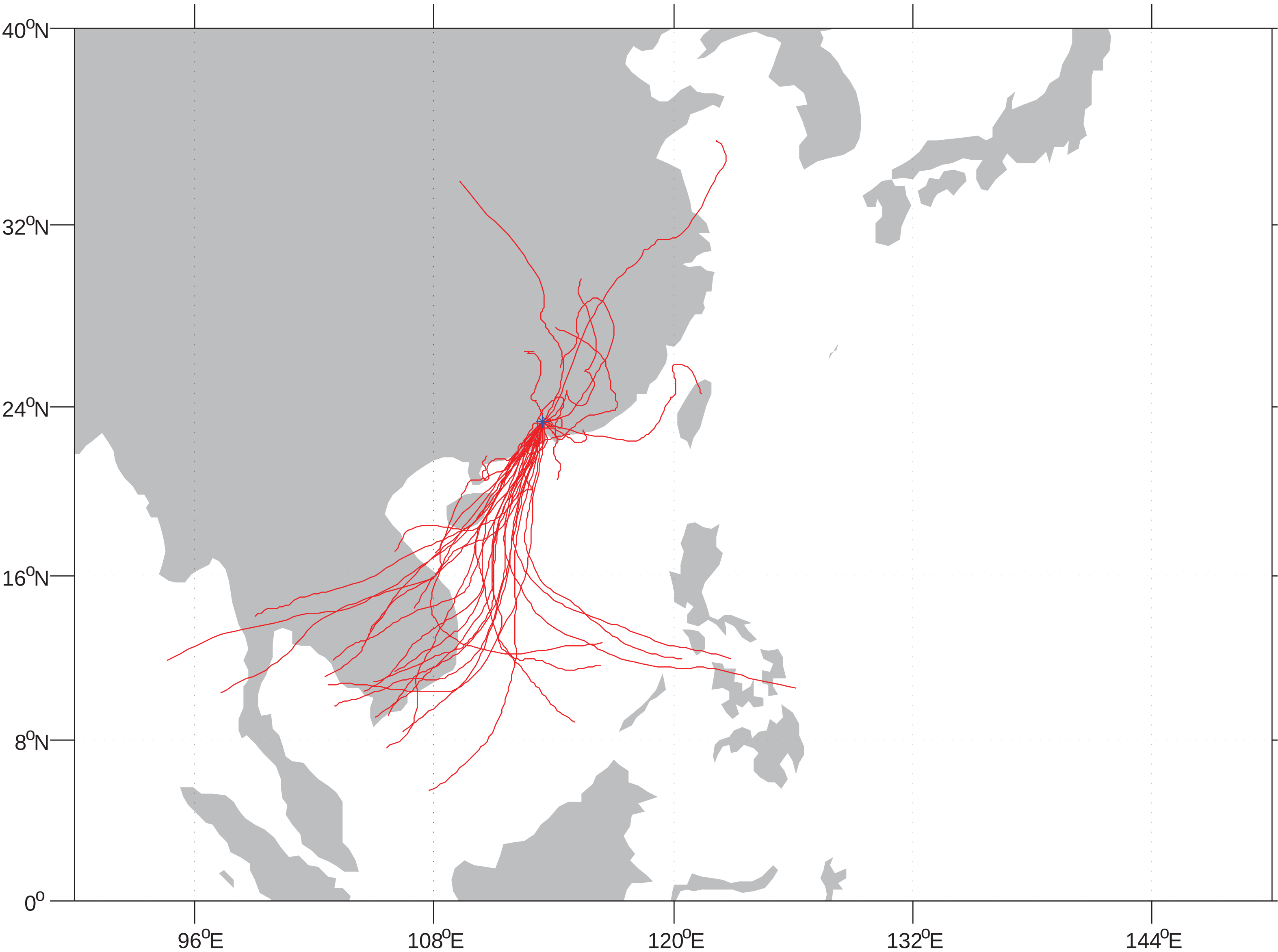

NC Rainy 1500m

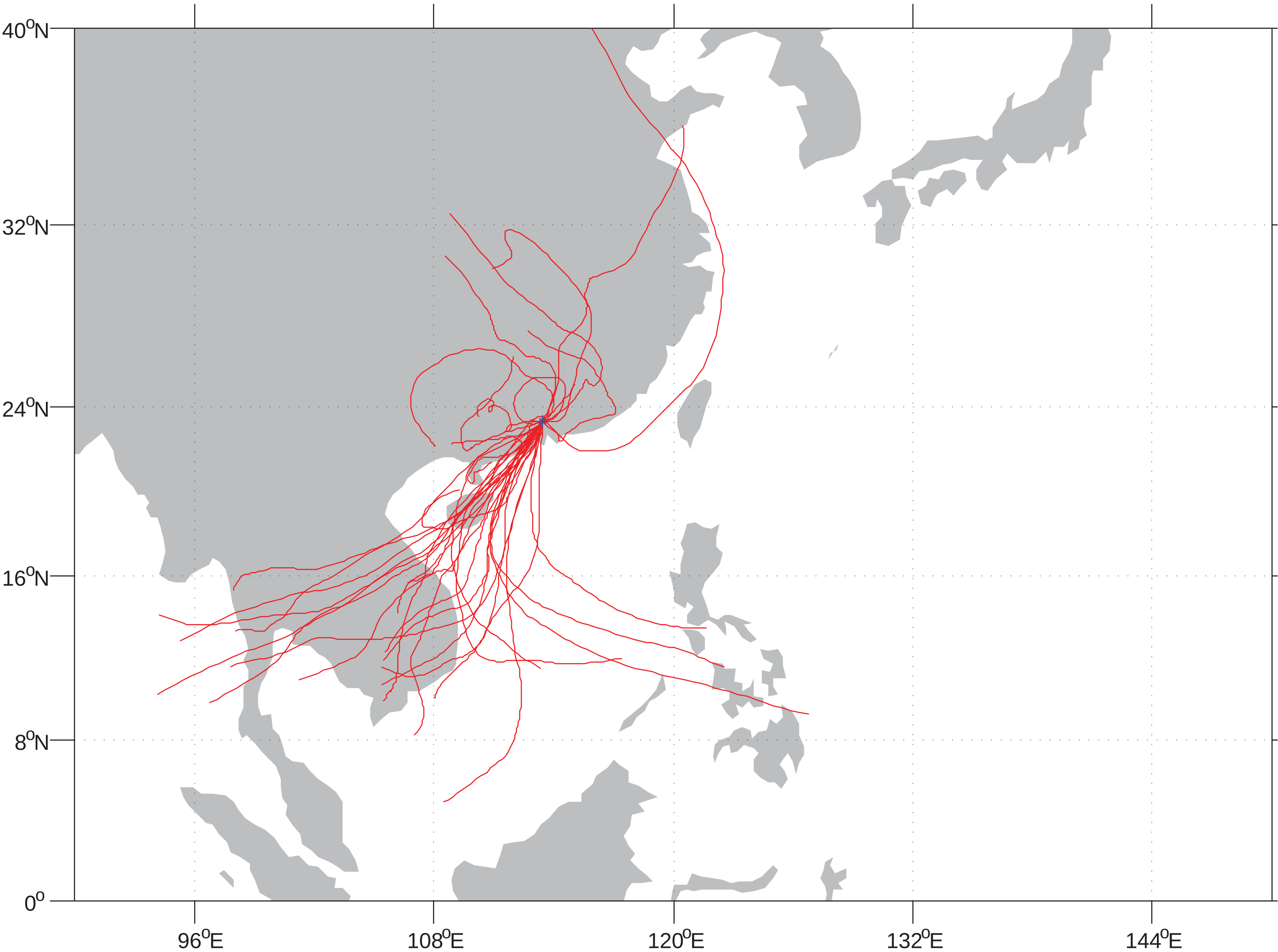

NC Dry 100m

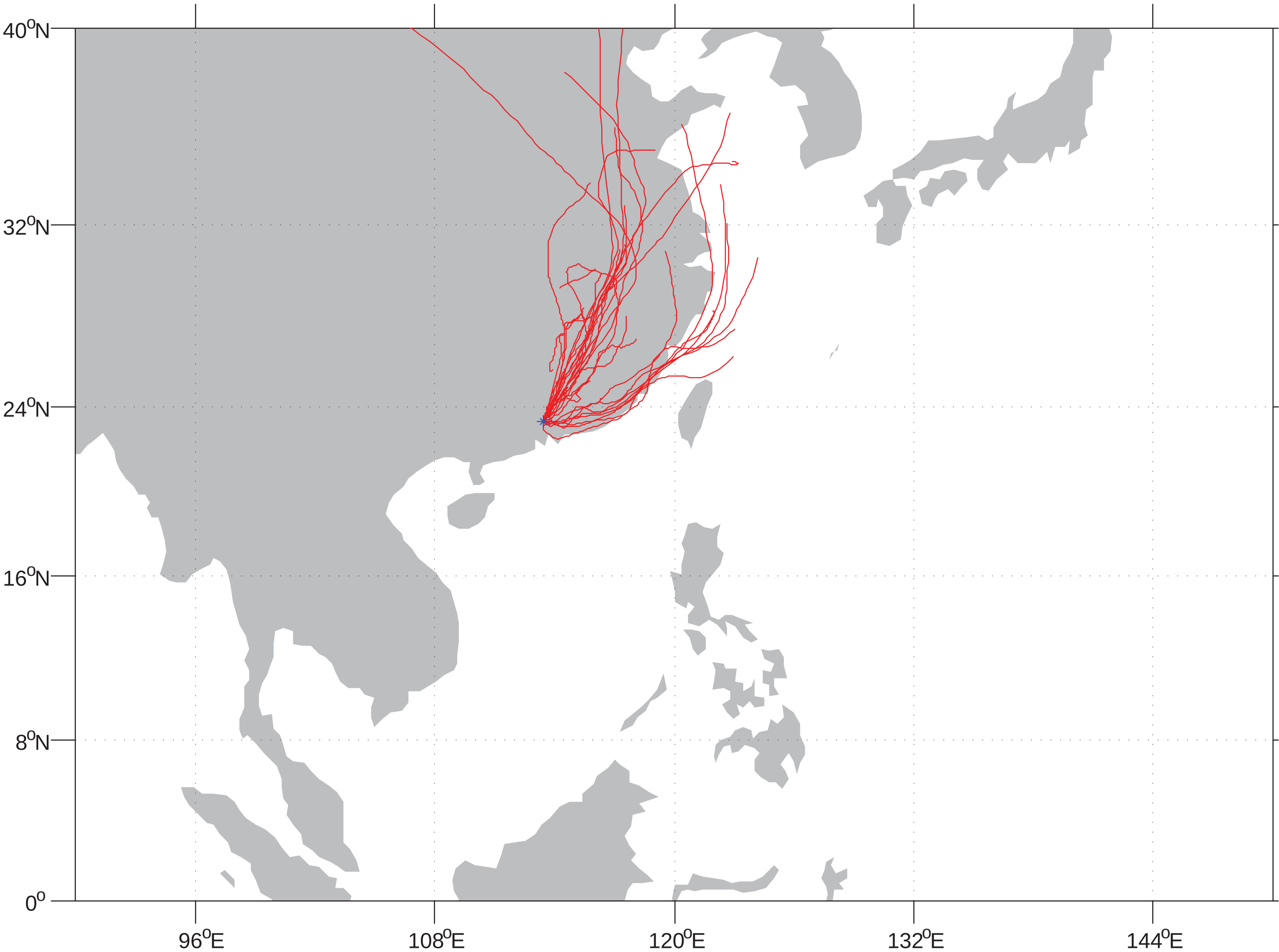

NC Dry 300m

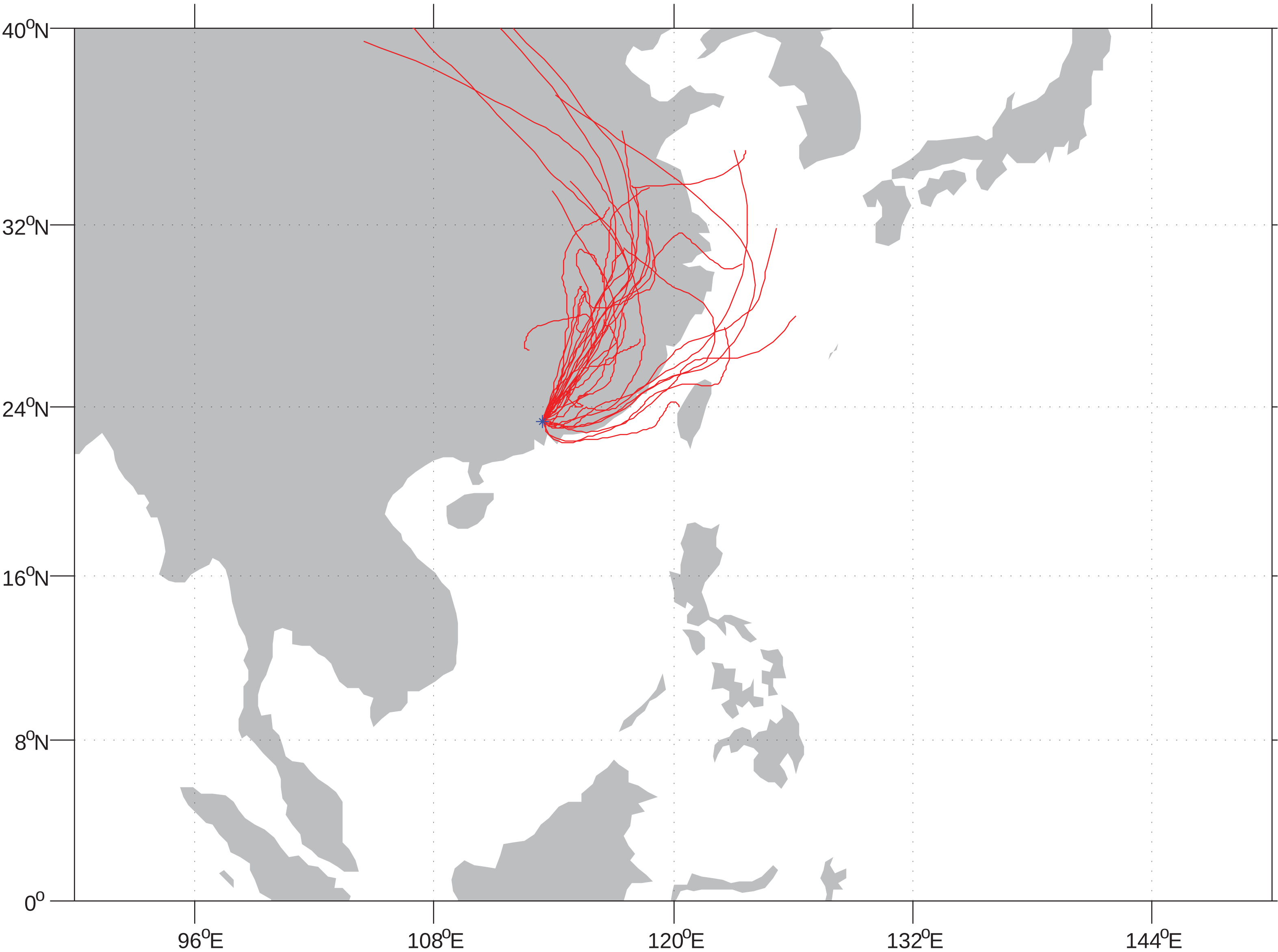

NC Dry 500m

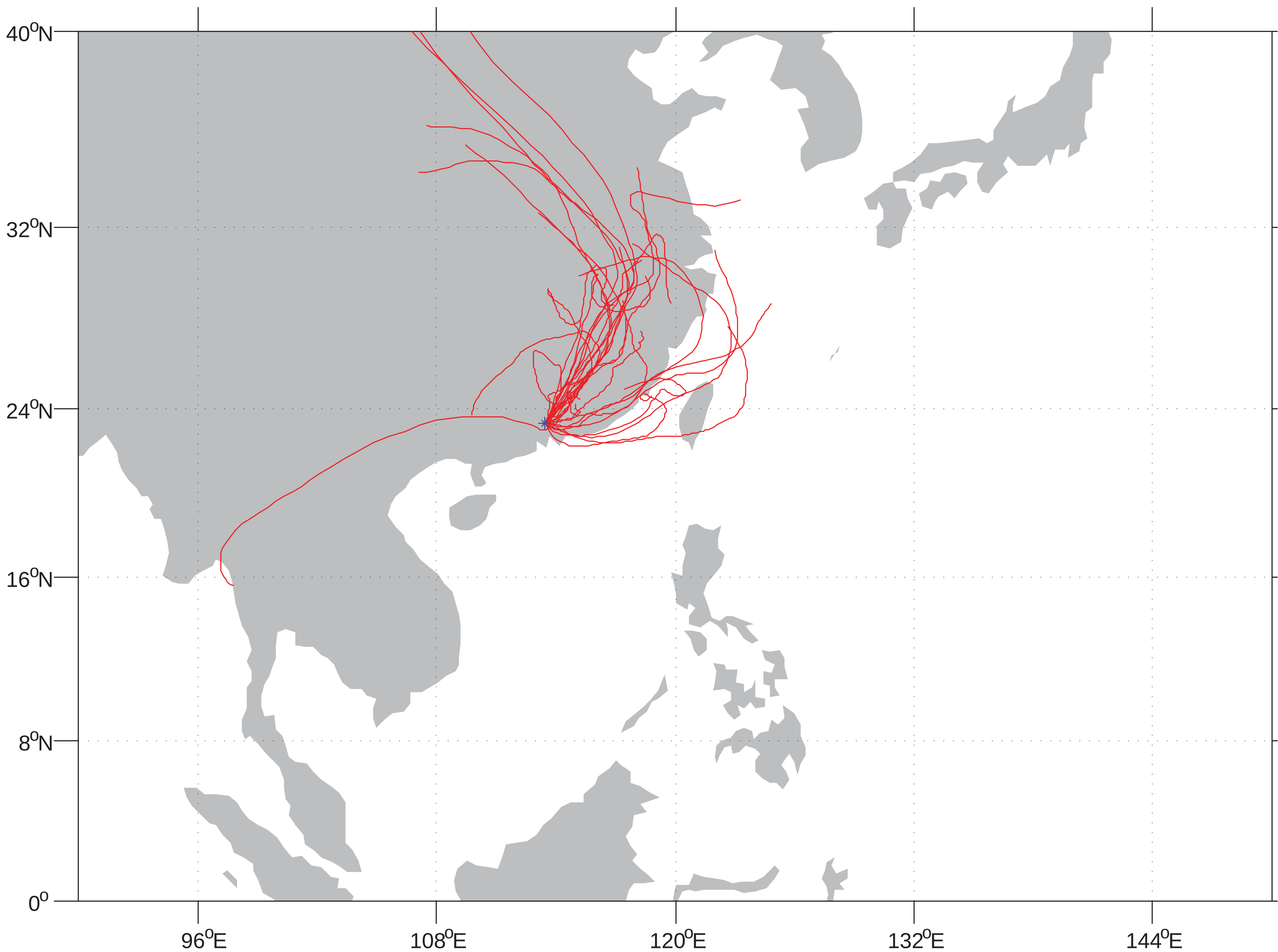

NC Dry 1000m

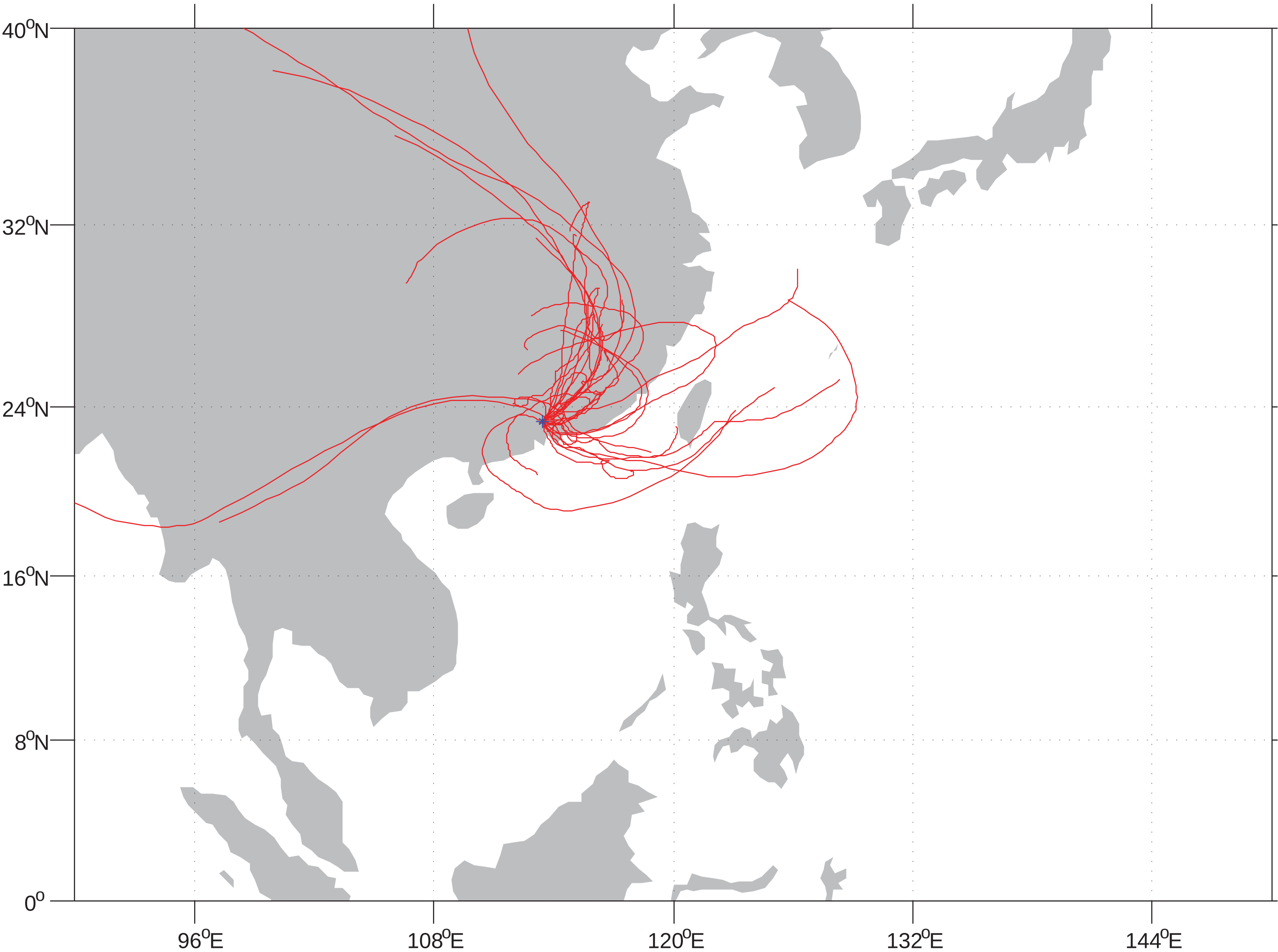

NC Dry 1500m

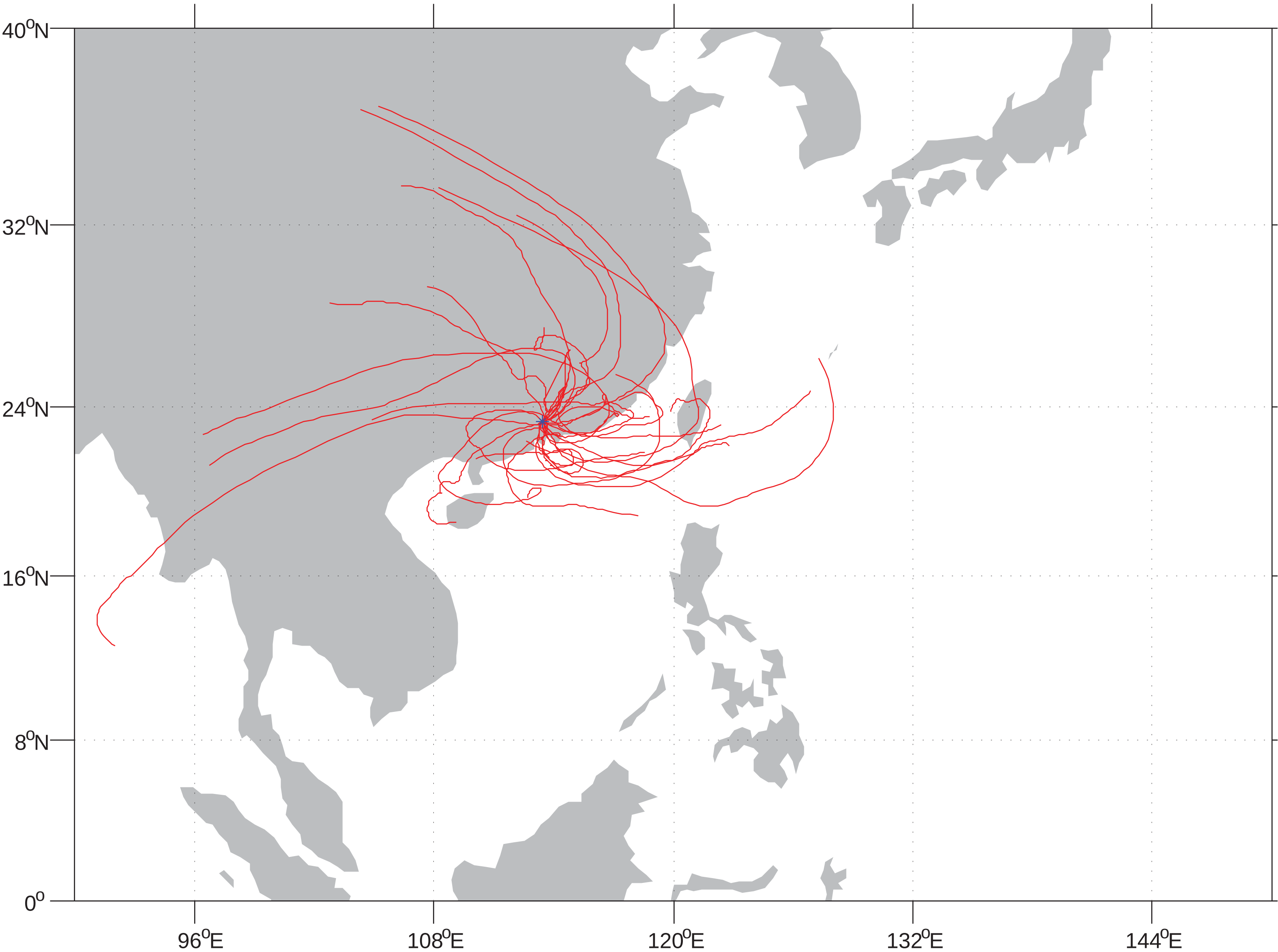

YX Rainy 100m

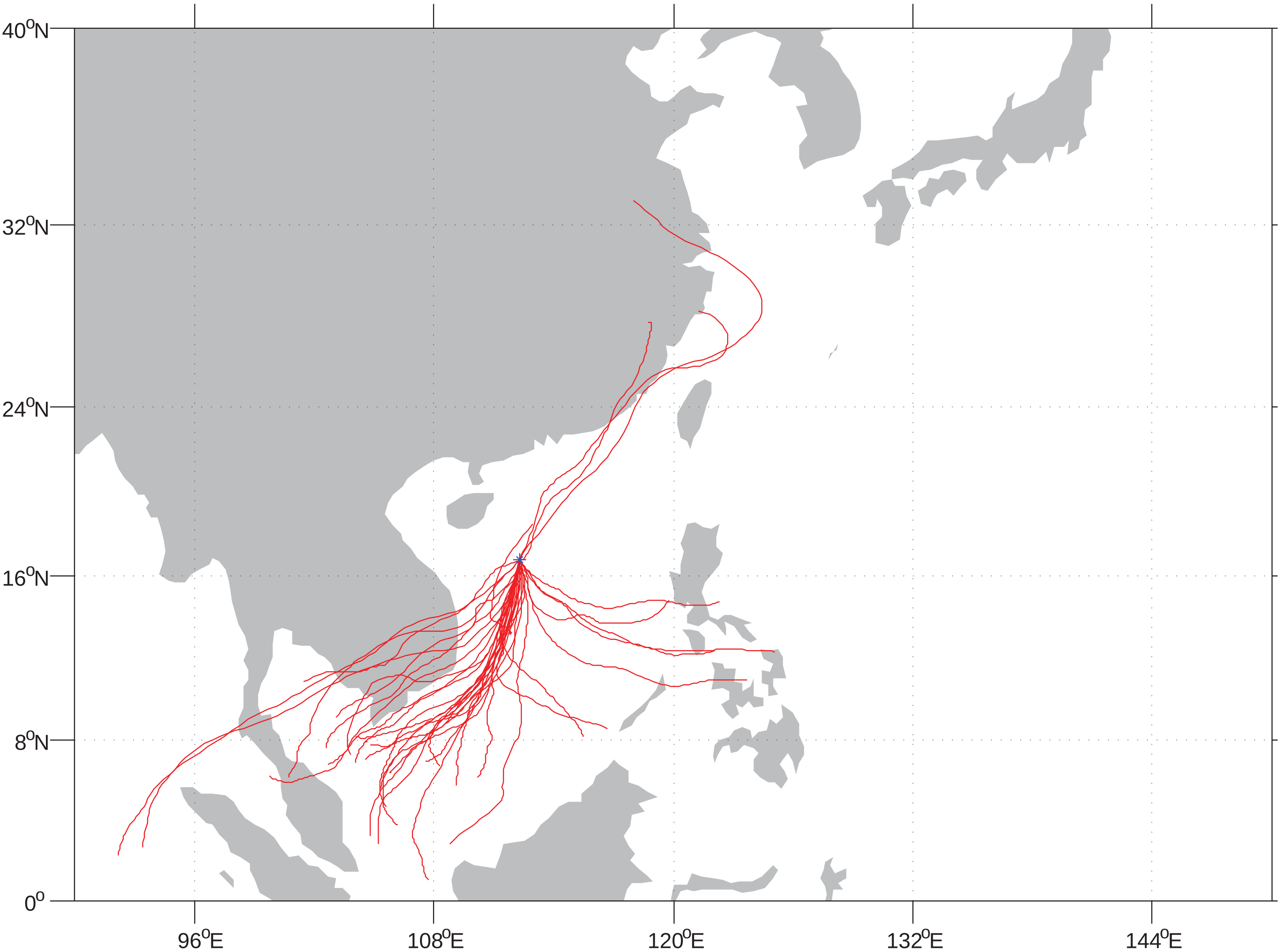

YX Rainy 300m

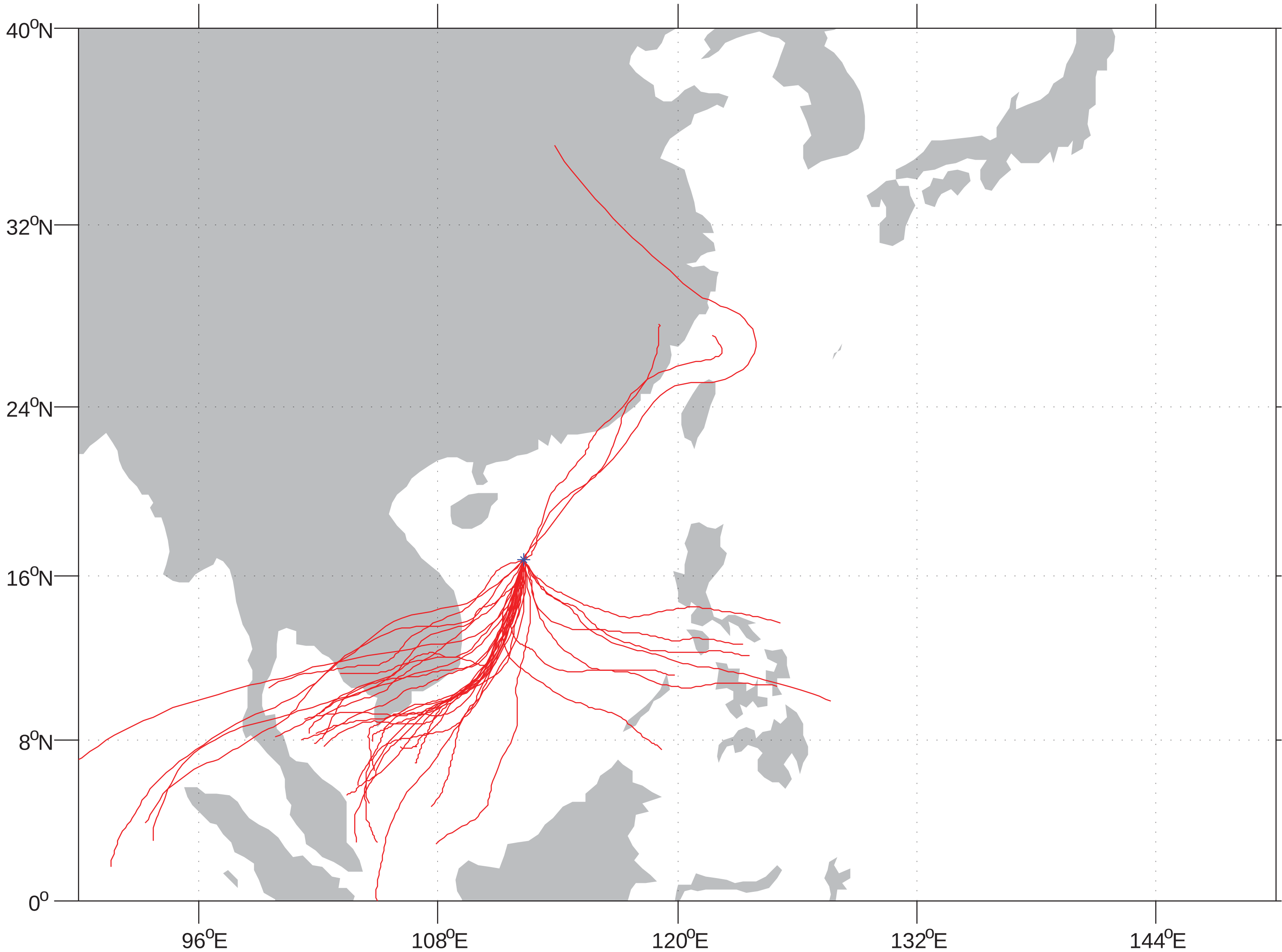

YX Rainy 500m

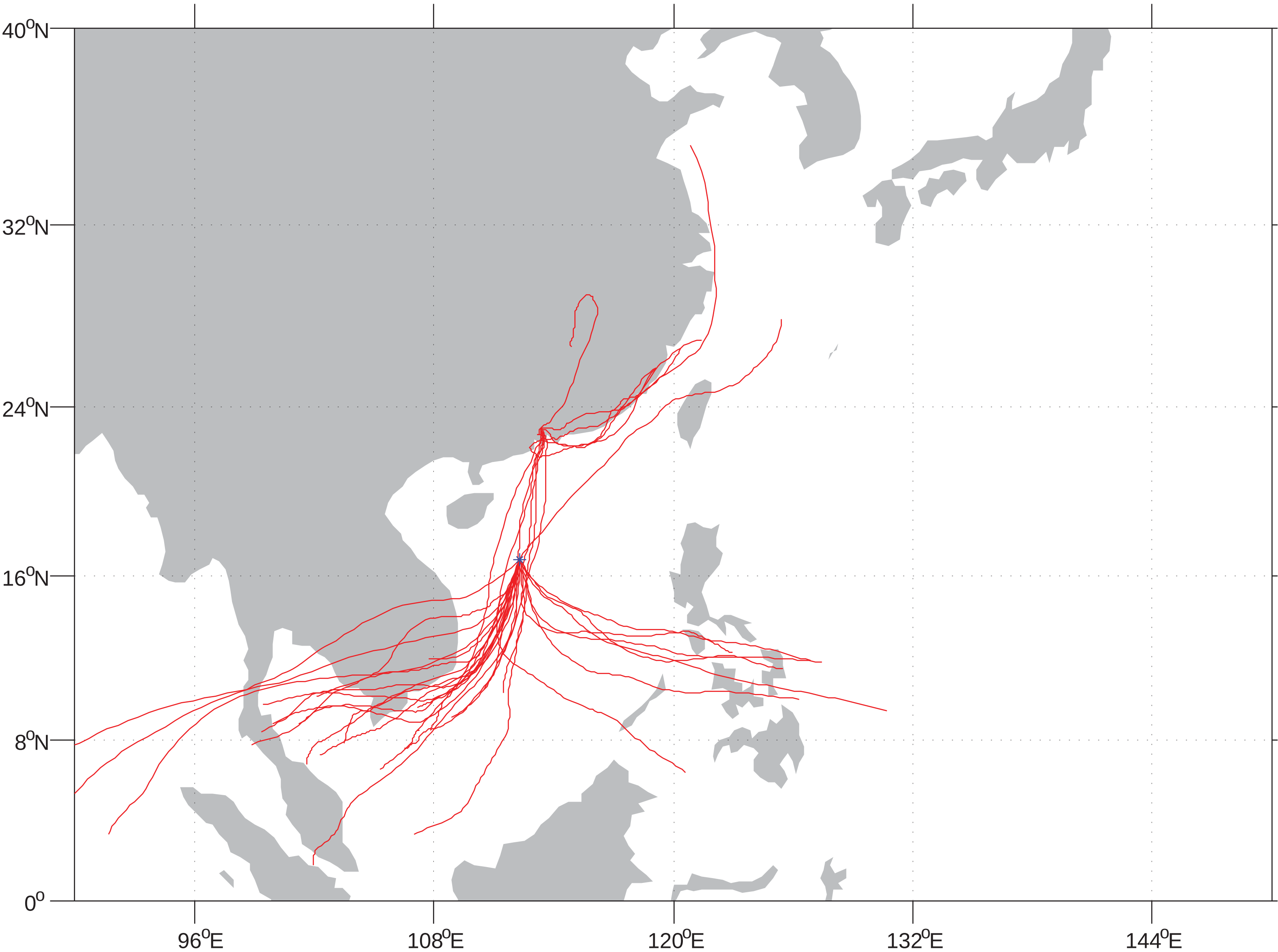

YX Rain 1000m

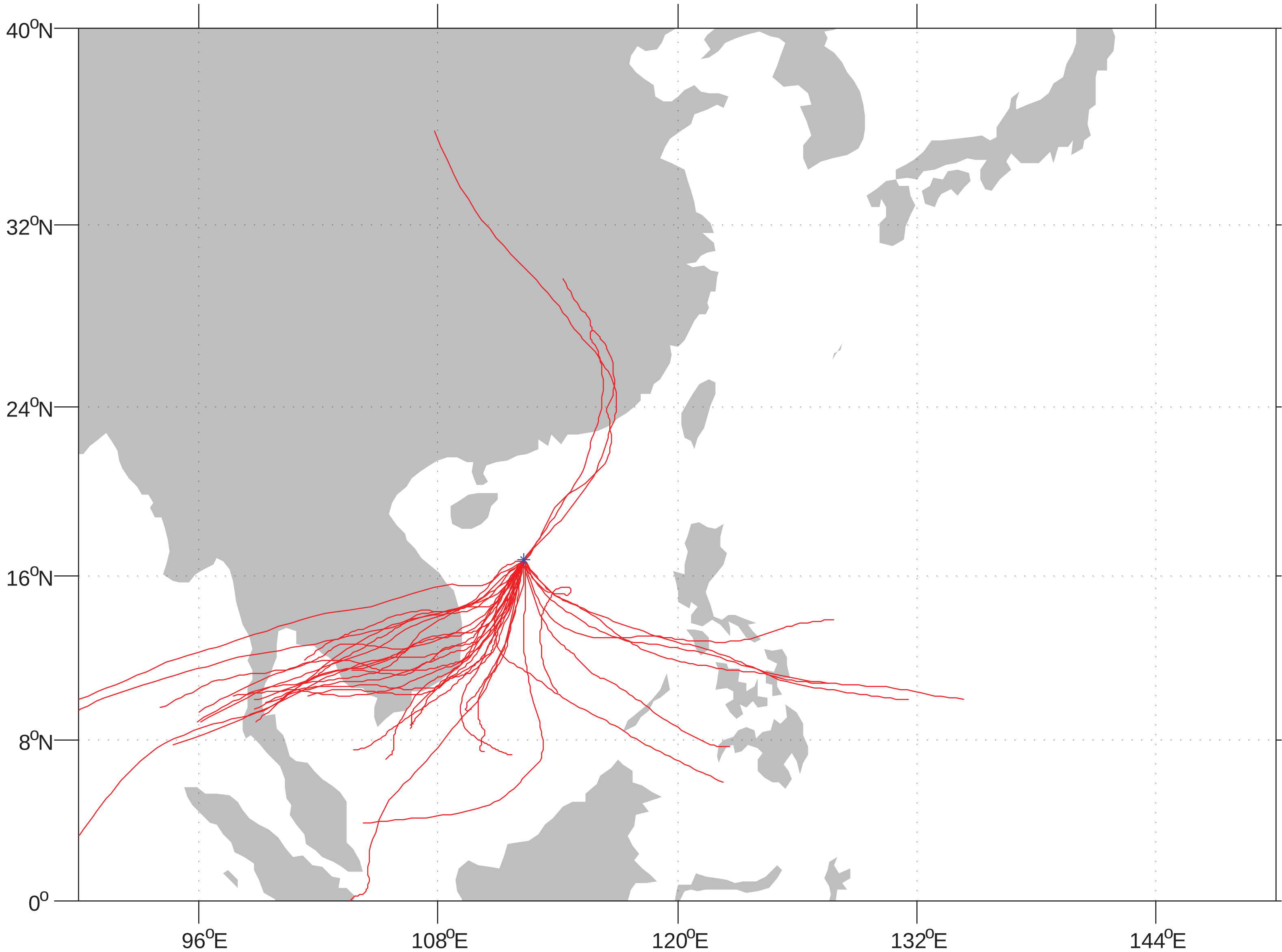

YX Rainy 1500m

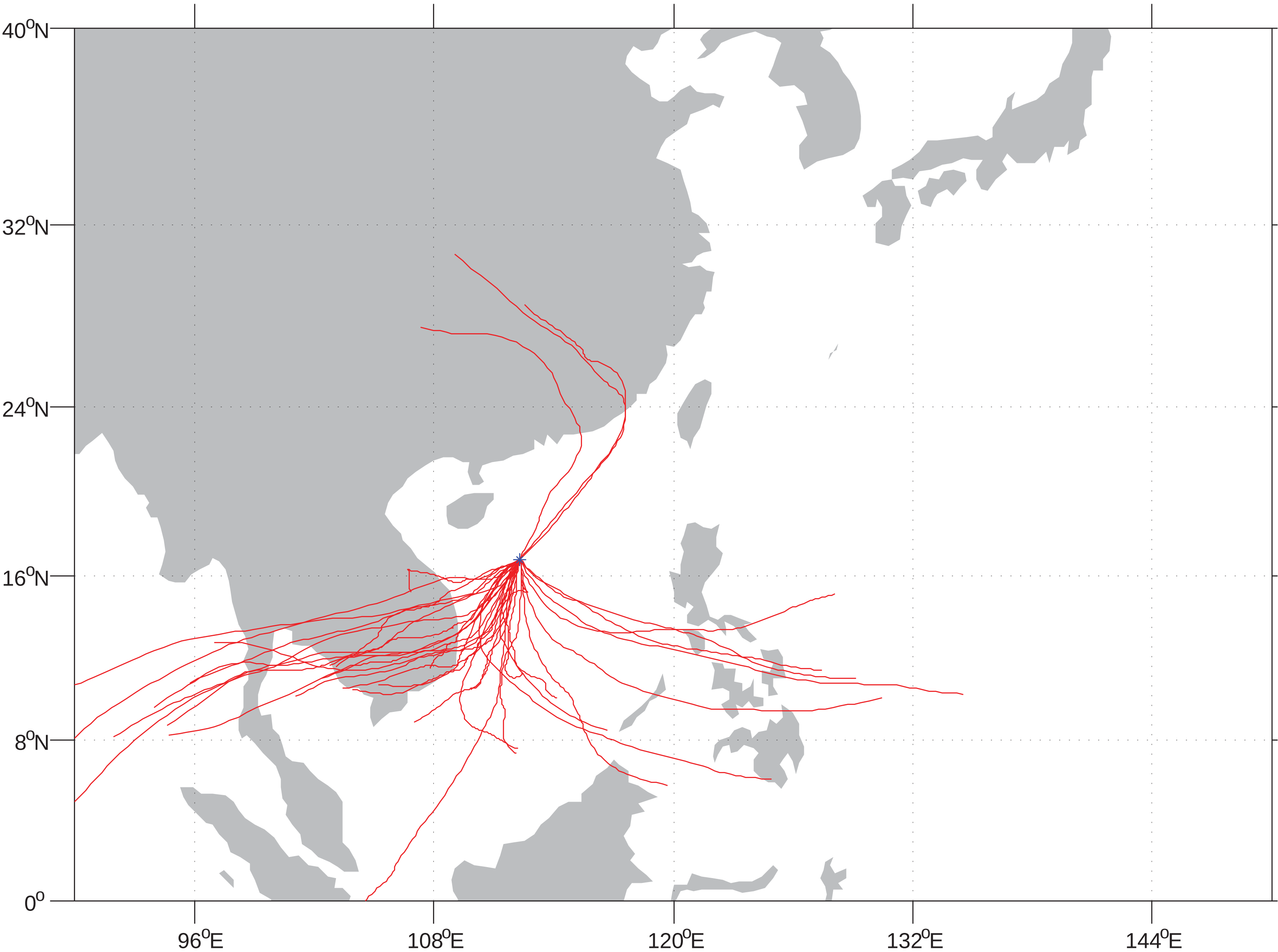

YX Dry 100m

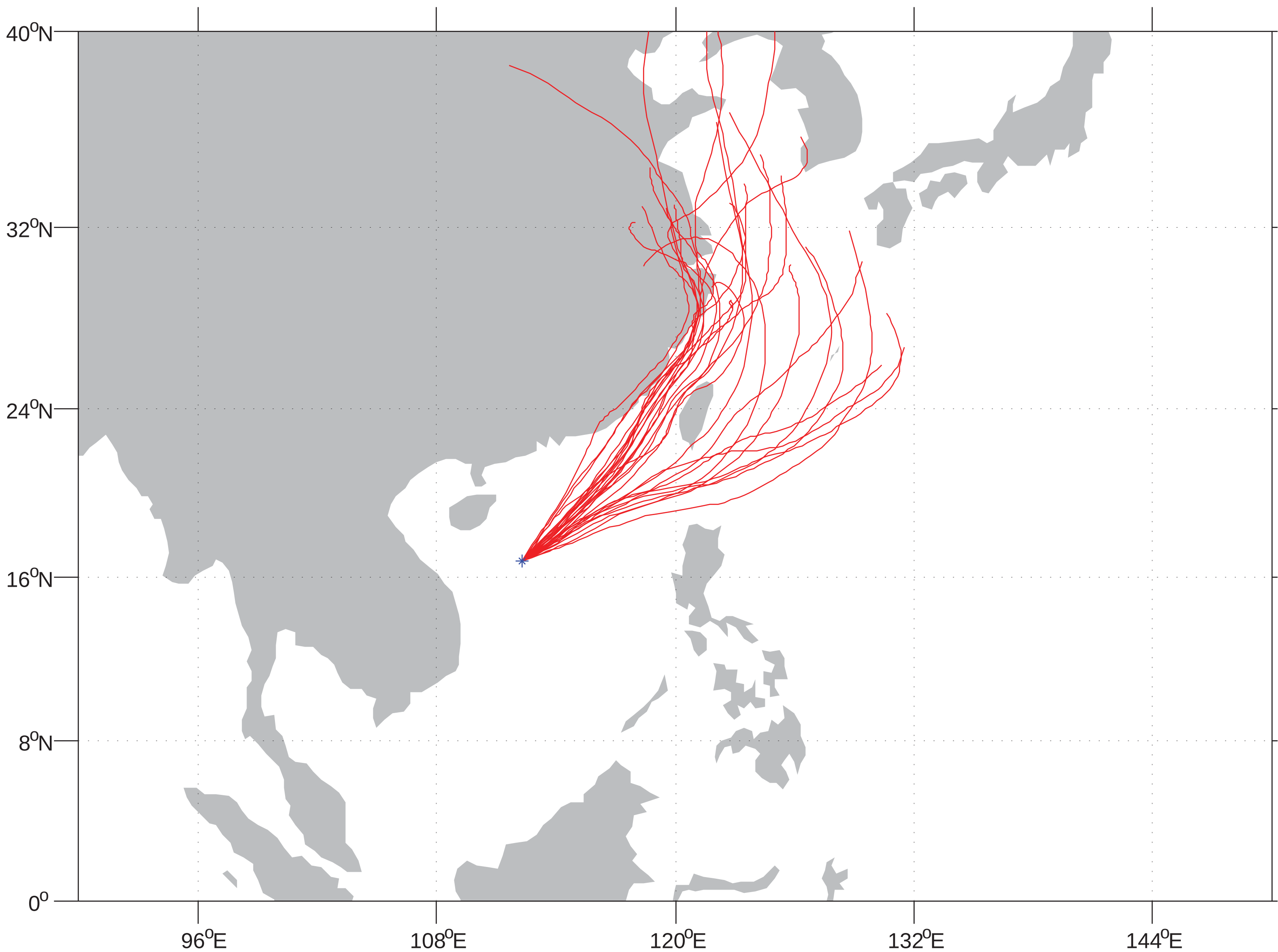

YX Dry 300m

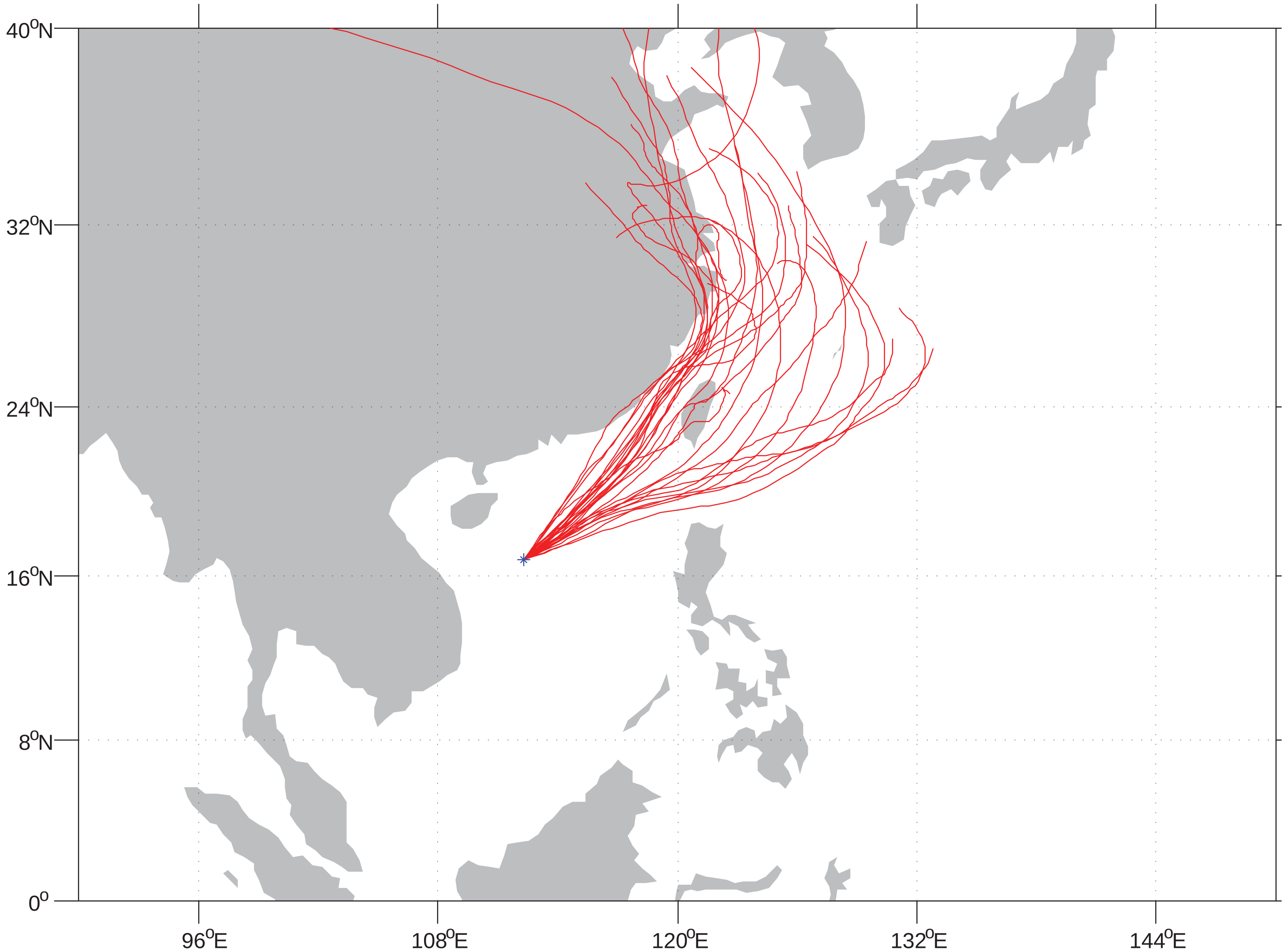

YX Dry 500m

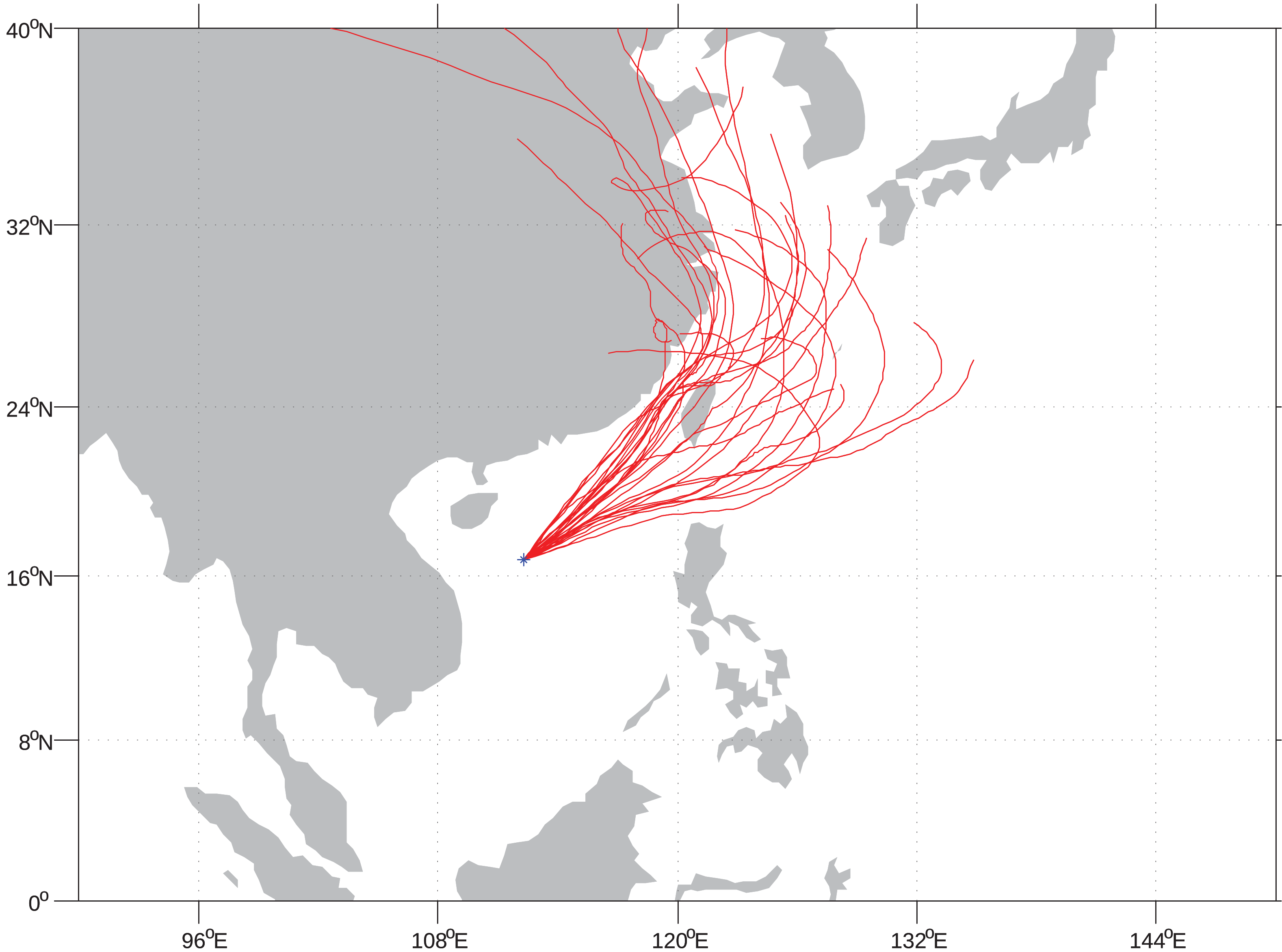

YX Dry 1000m

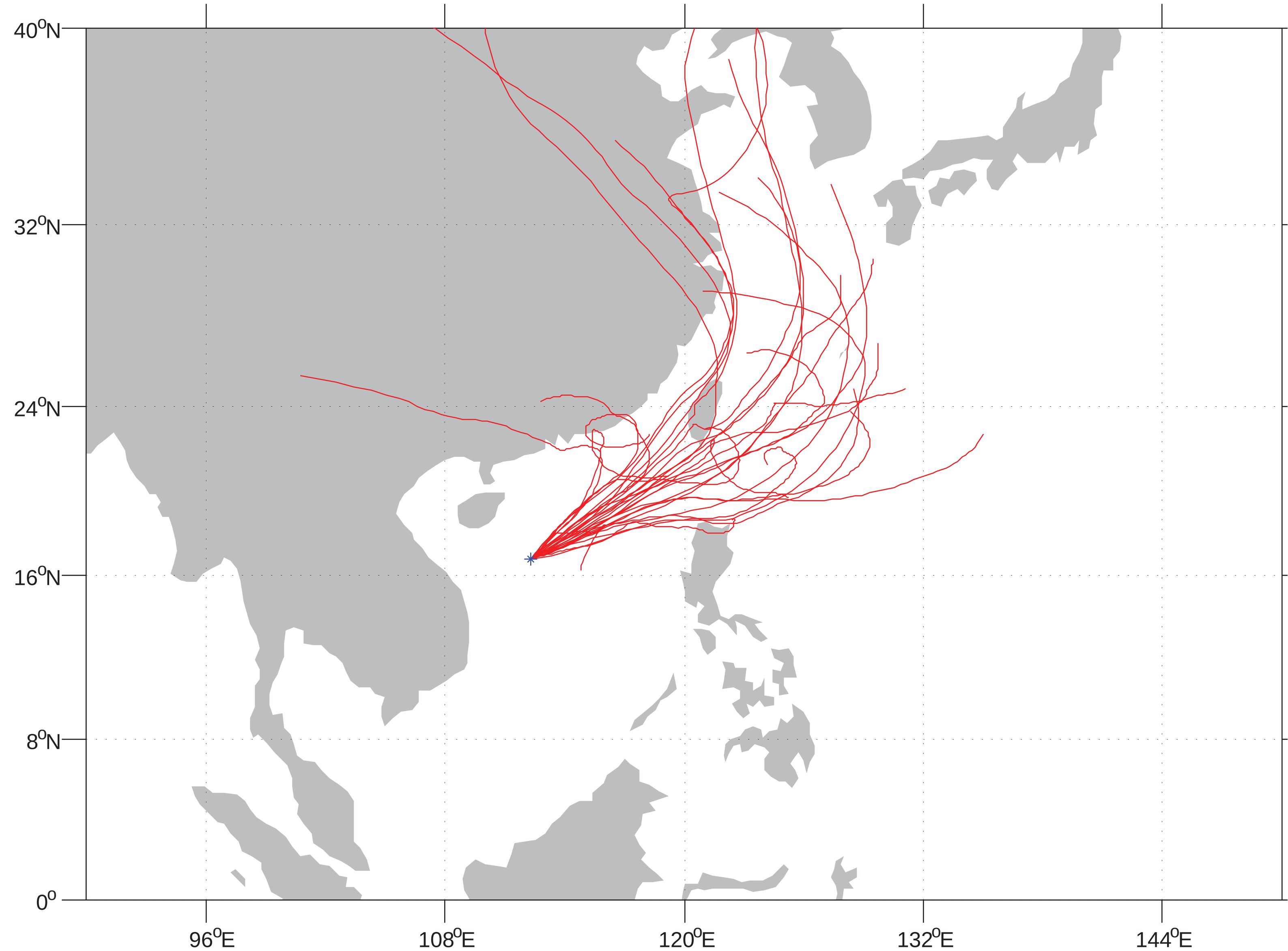

YX Dry 1500m

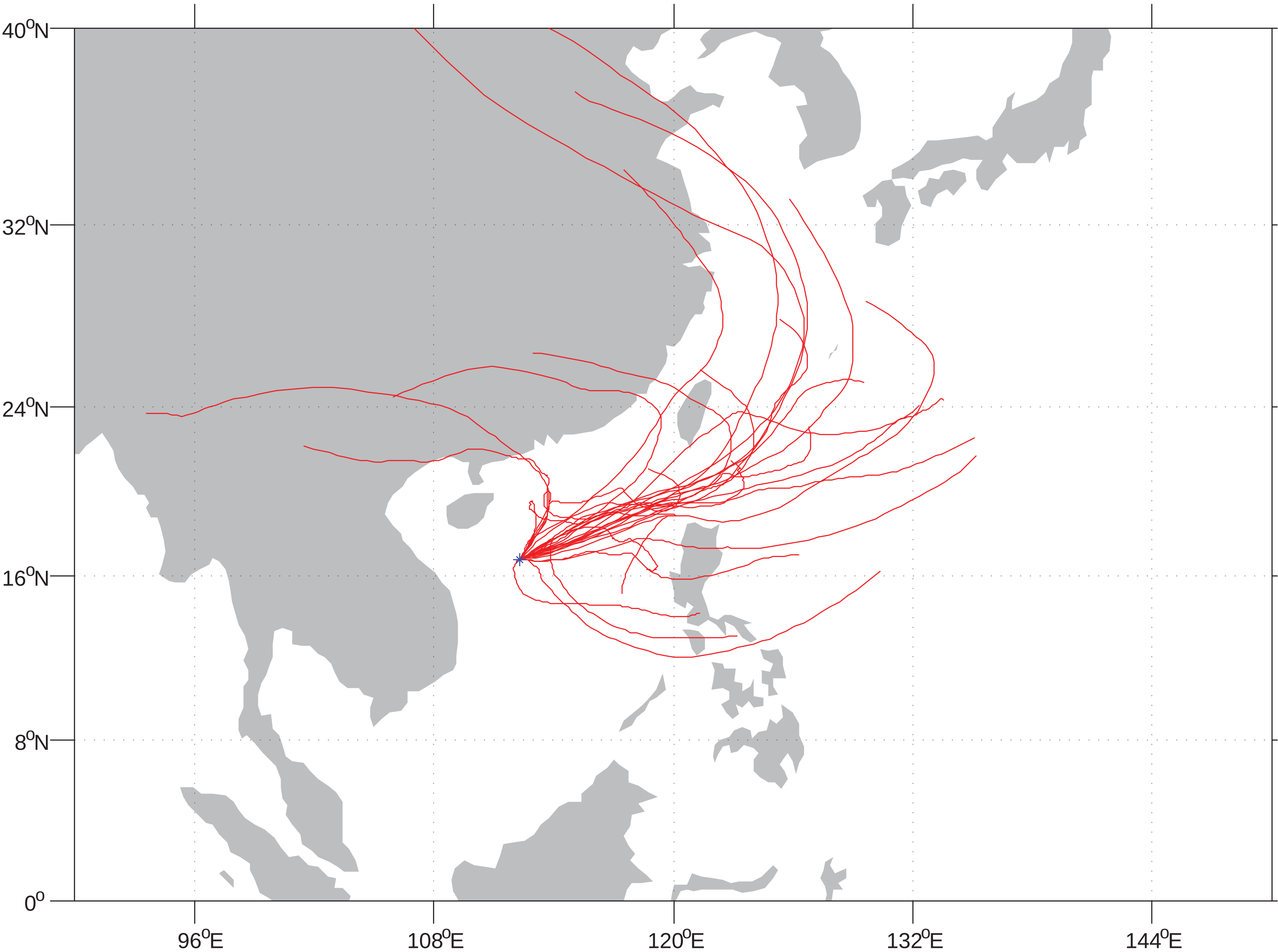

Table S1 Sampling site characteristics

Location	Type	Latitude	Longitude	Elevation (m)
Yongxing island (YX), SCS	Oceanic rural	16.83°N	112.33°E	5.6
Maofengshan (MFS), PRD	Rural	23.33°N	113.48°E	535
Nancun (NC), PRD	Suburban	23.00°N	113.35°E	141
Panyu (PY), PRD	Urban	22.93°N	113.32°E	12
Dongguan (DG), PRD	Suburban	22.97°N	113.73°E	43
Xinken, (XK), PRD	Rural	22.71°N	113.55°E	6.7
Yangshuo (YS), GX	Urban	24.77°N	110.50°E	75